UNIVERSIDAD DE CONCEPCIÓN

Centro de Investigación en Ingeniería Matemática (CI^{2}MA)

Well-balanced physics-based finite volume schemes for Saint-Venant-Exner-type models of sediment transport

Raimund Bürger, Enrique D. Fernández Nieto,
José Garres-Díaz, Jorge Moya

PREPRINT 2025-18

SERIE DE PRE-PUBLICACIONES

WELL-BALANCED PHYSICS-BASED FINITE VOLUME SCHEMES FOR SAINT-VENANT-EXNER-TYPE MODELS OF SEDIMENT TRANSPORT

RAIMUND BÜRGER[A], ENRIQUE D. FERNÁNDEZ-NIETO[B], JOSE GARRES-DÍAZ[C], AND JORGE MOYA[A,B,*]

Abstract. The Saint-Venant-Exner (SVE) model is widely used for the description of sediment transport including bedload, erosion, and deposition processes. A modified version of the SVE model, which includes sediment concentration incorporates exchange of sediment between the fluid and an erodible bed and a non-hydrostatic pressure for the fluid along with non-equilibrium entrainment and deposition velocities, is introduced. Gravitational effects on erosion are described by an effective shear stress formulation. This modified SVE model is derived from a general approach with density variations. It preserves the mass of both the sediment and the fluid, and satisfies a dissipative energy balance. On the other hand, well-balanced finite volume schemes adapted for SVE models are derived since standard well-balanced schemes for the Saint-Venant system with fixed bottom are in general no more well-balanced when applied to the SVE model. The latter property is due to the uncontrolled numerical diffusion associated with the bed evolution equation. Two novel techniques to achieve the well-balanced property for the modified SVE model are proposed. The first is a new polynomial-viscosity-matrix-based (PVM) scheme, denoted "PVM-2I", that modifies the numerical approximation of the bed evolution equation according to its related characteristic speed. The second is a physically motivated correction of the numerical diffusion term for the Rusanov and Harten-Lax-van Leer (HLL) schemes. The proposed schemes are positivity-preserving for the water height. Numerical solutions are compared with exact solutions with gravitational effects, with a novel exact solution in non-equilibrium conditions, and with experimental data. It is illustrated how the use of standard non-well-balanced schemes leads to a large artificial (unphysical) erosion and completely degraded solutions. This undesirable behaviour is avoided by the proposed well-balanced schemes.

1. Introduction

1.1. **Scope.** The dynamics of sediment transport is determined by the interplay between bedload, erosion, and deposition processes. While bedload involves the transport of sediment particles captured in an erodible bottom, erosion refers to the entrainment of sediment into the fluid, and deposition occurs when sediment particles settle back onto the bed. These processes affect sediment transport rates, which in turn influence river morphology and sediment distribution. Accurate modelling of these processes requires the formulation of appropriate deposition rates, settling velocities, and sediment entrainment factors. The Saint-Venant-Exner (SVE) system is widely used to describe bedload sediment transport. It combines the Saint-Venant (or shallow water) system

Date: September 24, 2025.

Key words and phrases. Finite volume method, depth-averaged model, well-balanced methods, sediment transport.

*Corresponding author.

[A]CI^{2}MA and Departamento de Ingeniería Matemática, Facultad de Ciencias Físicas y Matemáticas, Universidad de Concepción, Casilla 160-C, Concepción, Chile. E-Mail: rburger@ing-mat.udec.cl, jorgemoya@udec.cl.

[B]Departamento de Matemática Aplicada I & IMUS, ETS Arquitectura, Universidad de Sevilla, Avda. Reina Mercedes No. 2, 41012 Sevilla, Spain. E-Mail: edofer@us.es, jmoya1@us.es.

[C]Departamento de Matemática Aplicada II & IMUS, ETS Ingeniería, Universidad de Sevilla, Camino de los Descubrimientos s/n, 41092 Sevilla, Spain. E-Mail: jgarres@us.es.

for hydrodynamics with a continuity equation (the Exner equation) to model the bed evolution. Furthermore, erosion and deposition are commonly described by empirical formulas.

The Exner equation [15] defines sediment transport in terms of the solid transport discharge, which requires specifying a model closure. For this purpose, several empirical models have been introduced, although they often lack dissipative energy properties and/or violate mass conservation. Moreover, many of these models are only validated for nearly horizontal sediment beds, which is also a major limitation. Several SVE-type models have been formulated in terms of the closure of the solid transport discharge. Well-known choices include the Meyer-Peter and Müller [27] or Ashida-Mishiue [3] solid transport discharge closures. These models are also defined under the assumption of a small slope of the bottom and do not account for gravitational effects. Furthermore, these models assume an equilibrium between erosion and deposition rates, as well as small interactions between the fluid and sediment layers. As a consequence, SVE models that are based on such a definition of solid transport discharge do not satisfy an associated energy balance.

Fernández-Nieto et al. [16] formally deduced SVE models from an asymptotic analysis of a coupled system with the shallow water system and a Reynolds equation. The models proposed in [16] take into account gravitational effects and include several versions with equilibrium or non-equilibrium assumptions. Moreover, they are endowed with an associated energy balance. In [19], a specific semi-implicit numerical method for the model introduced in [16] in equilibrium conditions is introduced. That method is designed for subcritical flows. The difficulty relies in the nonlinear degenerate parabolic behaviour of the gravitational terms in the solid transport discharge. To overcome this difficulty, a particular formulation of the solid transport discharge suitable for the application of a semi-implicit numerical discretization is introduced in [19]. This formulation will be used here.

Shallow water systems, which usually form the hydrodynamic part of sediment transport models, are typically based on a hydrostatic framework for the fluid, which means that vertical acceleration and dispersive effects are neglected. Nevertheless, non-hydrostatic pressure may strongly influence the fluid dynamics, as it is shown in several studies of depth-averaged models (see e.g. [4, 36, 32, 37] and references cited in these works). Roughly speaking, these models form two big families, namely Boussinesq-type and non-hydrostatic models, although many of them may be rewritten in both formulations (see [13]). The main difference is that dispersive Boussinesq-type models introduce high-order derivatives to account for dispersive effects, whereas the so-called non-hydrostatic models incorporate new unknowns and additional equations. This property simplifies the numerical approximation since only first-order derivatives appear (see e.g. [14, 17, 38]).

Numerical approximations of SVE-type models formulated as hyperbolic systems of first-order partial differential equations are usually based on finite volume (FV) methods. In the context of geophysical flows, these systems frequently include non-conservative products, which complicate the application of standard FV schemes. A widely studied problem of this kind is the incorporation of an erodible or fixed bottom into the shallow water equations. A well-known class of FV schemes that properly handle non-conservative products are the so-called path-conservative schemes [10, 28, 35]. These schemes have been successfully applied to hyperbolic systems with non-conservative products in many applications, including multilayer shallow water systems, compressible gas dynamics, or magnetohydrodynamics. Furthermore, Parés and Castro [29] proposed a generalization of the Roe method (see also [35]). However, its implementation requires explicit knowledge of the eigenstructure of the intermediate matrices. To overcome this limitation, Castro and Fernández-Nieto [11] introduced a specific family of path-conservative schemes, named polynomial viscosity matrix (PVM) methods, which extend many FV schemes based on incomplete Riemann solvers such as the Lax-Friedrichs scheme, the Rusanov scheme (also called local Lax-Friedrichs (LLF) scheme, [24])

and the Harten-Lax-van Leer (HLL) scheme [23]. One of the difficulties of designing such schemes is related to the well-balance property, which refers to the ability of the scheme to preserve certain stationary solutions, in particular, the steady at rest (or water at rest) solutions, i.e., flat free surface and zero velocity. For a fixed bottom, numerous schemes are well-balanced. However, if one of these schemes (that are well-balanced for a fixed bottom) is used to solve the SVE equations then its steady solutions will not be preserved in many cases, even in the case of no fluid velocity and zero solid transport discharge, because the bed sediment will move continuously. This unphysical behaviour comes from uncontrolled numerical diffusion in the discretization of the bed evolution equation within the SVE model; this problem does not arise in the case of a fixed bottom (see [25]).

In this work, we introduce a modified SVE-type model that is deduced from a general model with density variation and a Boussinesq-type assumption to account for all these effects. Specifically, the model includes a non-hydrostatic pressure for the fluid layer, gravitational effects, and sediment in suspension. Each of these effects can be activated or deactivated as needed. Furthermore, a general formulation for the solid transport discharge in the sediment layer makes it possible to formulate this simplified model in equilibrium (erosion rate equals deposition rate) or non-equilibrium conditions. Moreover, an energy balance implies that under appropriate boundary conditions, the contributions of energy are controlled by dominantly dissipative mechanisms. Another contribution is a novel time-dependent semi-analytical solution for the non-equilibrium model used to validate the methods proposed. The principal novelty, however, are two new techniques to achieve the well-balance property of schemes for the general SVE-type model: firstly, a scheme, denoted here by PVM-2I, which coincides with the HLL scheme for the flow variables but modifies the numerical approximation of the bed evolution equation according to its related characteristic speed; and secondly, a physically motivated correction of the numerical diffusion term for Rusanov and HLL schemes. To our knowledge, no technique in the literature has been presented thaty would be well-balanced for Rusanov and HLL-type methods for SVE models. As mentioned, Rusanov and HLL methods can be expressed as PVM methods involving constant and linear polynomials of the system matrix. An advantage of these methods is their preservation of the positivity of the water depth (see [5]). On the contrary, PVM methods including a second-order term, which includes a square of the system matrix, present challenges in proving positivity. As a consequence, the well-balanced Rusanov and HLL methods proposed in this paper are excellent candidates to be considered as basal schemes for the development on high-order well-balanced FV method based on reconstructed states. Gravitational terms are discretized by following the approach of [19] not only in subcritical flows but also in supercritical regimes.

1.2. **Outline of the paper.** The remainder of this work is organized as follows. Section 2 is dedicated to the derivation and definition of the model, along with the analysis of its key properties. The proposed model describes bedload transport and the interaction between fluid and sediment through the processes of erosion and deposition of suspended particles. First, in Section 2.1 the balance equations are formulated. These describe conservation of mass and linear momentum, sediment transport, and bed evolution. The resulting balance equations are supplemented by an incompressibility condition. In Section 2.2 the bedload flux is defined for several cases including non-equilibrium and equilibrium models with and without gravitational effects. Bedload discharge represents the quantity of sediment particles transported along the riverbed or channel per unit time. Next, in Section 2.3 we verify that the model complies with mass conservation. Then, in Section 2.4 we demonstrate that the total mechanical energy of the model satisfies a dissipative energy balance. Section 3 focuses on the numerical approximation of the model, including the treatment of source terms coming form the erosion and deposition rates, non-hydrostatic pressure,

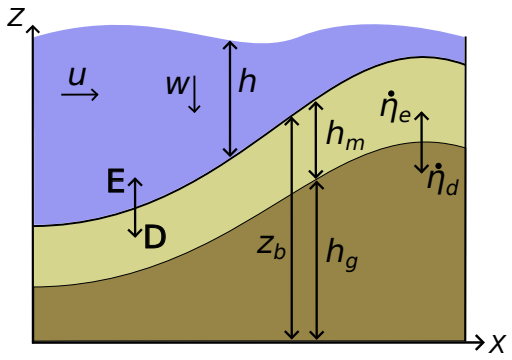

FIGURE 1. Schematic representation of the proposed model, illustrating key variables such as the water depth h, sediment concentration c, and the height of the erodible bed z_b composed of an active layer h_m and a fixed layer h_g, see Table 1.

and gravitational effects. To this end, we introduce in Section 3.1 some preliminaries and outline in Section 3.2 the finite volume method for the governing hyperbolic system with non-conservative products. The main contributions of this paper are in Sections 3.3 and 3.4 where the well-balanced corrections for Rusanov and HLL methods, and the new PVM-2I method, are presented. Furthermore, in Section 3.5 we introduce a semi-implicit numerical scheme to handle gravitational terms that influence the vertical motion of particles, particularly their settling and redistribution. The semi-implicit treatment enhances stability while maintaining computational efficiency. Next, in Section 3.6 we deal with the source terms related to erosion and deposition, and conclude the formulation of the scheme with description of the projection method to handle the non-hydrostatic pressure (Section 3.7). Section 4 is devoted to the numerical tests. We validate our numerical schemes through a series of test cases, including semi-analytical solutions, academic test, and comparisons with experimental data. Here, various simplified cases are considered, such as the case to consider or not sediment in suspension, equilibrium and non-equilibrium models and the influence of gravitational effects. In particular, we illustrate the well-balancedness of the proposed method and the accuracy of the PVM-2I scheme with respect to the Rusanov and HLL methods due to the reduction of numerical diffusion for the bed evolution equation. Finally, in Section 5 we summarize our findings.

2. Model of sediment transport with suspended with particles

The framework of the sediment transport model is sketched in Figure 1. A central feature of the model is the inclusion of the so-called active layer, which refers to the uppermost portion of the erodible bed that directly interacts with the overlying flow. This layer is characterized by the continuous exchange of sediment particles via entrainment and deposition. This process plays a crucial role in controlling the short-term dynamics of sediment transport. Typically, the active layer has a finite thickness and consists of grains that are more mobile than those in the underlying layer [16].

TABLE 1. Definition of key variables associated to Figure 1.

Symbol	Description
h	water depth
u, w	horizontal and vertical velocities
c	sediment concentration
z_b	position of erodible bed
h_g	fixed bed level
E, D	sediment erosion (E) and deposition (D) rates
$\dot\eta_\mathrm{e}, \dot\eta_\mathrm{d}$	entrainment and deposition velocities
ρ_f	density of fluid
ρ_s	density of sediment
ψ_0	porosity
$r_\mathrm{s} = \rho_\mathrm{s}/\rho_\mathrm{f}$	sediment-fluid density ratio
$\rho_0 = \psi_0\rho_\mathrm{f} + (1-\psi_0)\rho_\mathrm{s}$	bulk density of the mixture
$\rho = c\rho_\mathrm{s} + (1-c)\rho_\mathrm{f}$	mixture density
$\hat p_\mathrm{nh}$	non-hydrostatic pressure
p_nh	$\hat p_\mathrm{nh}/\rho$
τ	friction law (Manning or Darcy-Weisbach)

2.1. **Balance equations.** In Table 1 we indicate the variables that are used. With these definitions, the governing equations in the non-hydrostatic case are given by

$$\partial_t(h\rho) + \partial_x(h\rho u) = \rho_0\frac{E-D}{1-\psi_0}, \tag{2.1}$$

$$\partial_t(h\rho u) + \partial_x\left(h\rho u^2 + \frac{1}{2}gh^2\rho + h\hat p_\mathrm{nh}\right) = -(\rho gh + 2\hat p_\mathrm{nh})\partial_x z_\mathrm{b} - \tau + \frac{u}{2}\rho_0\frac{E-D}{1-\psi_0}, \tag{2.2}$$

$$\partial_t(h\rho w) + \partial_x(h\rho uw) = 2\hat p_\mathrm{nh} + \frac{w}{2}\rho_0\frac{E-D}{1-\psi_0}, \tag{2.3}$$

$$\partial_t(hc) + \partial_x(huc) = E - D, \tag{2.4}$$

$$\partial_t z_\mathrm{b} + \frac{1}{1-\psi_0}\partial_x q_\mathrm{b} = -\frac{E-D}{1-\psi_0}, \tag{2.5}$$

$$\partial_t h_\mathrm{g} = -(\dot\eta_\mathrm{e} - \dot\eta_\mathrm{d}). \tag{2.6}$$

The specific definitions of E, D, $\dot\eta_\mathrm{e}$, and $\dot\eta_\mathrm{d}$ are provided in Section 2.2. The quantity $\hat\tau$ is introduced in Section 2.4. Equations (2.1)–(2.4) describe conservation of mass and momentum, (2.5) models sediment transport, and (2.6) describes bed evolution. The last terms on the right-hand side of (2.2) and (2.3) describe the transfer of linear momentum between the fluid and sediment layers. Equations (2.1) to (2.6) are supplemented by the incompressibility condition

$$w - u\partial_x z_\mathrm{b} + \partial_t z_\mathrm{b} + \frac{h}{2}\partial_x u = 0.$$

The system (2.1)–(2.3) may be rewritten in terms of the unknowns h, hu, and hw. First, combining (2.1) and (2.4), we get

$$\partial_t h + \partial_x(hu) = \frac{E-D}{1-\psi_0}.$$

Using this equation we obtain the momentum balance equations for hu and hw

$$\begin{aligned}\partial_t(hu)+\partial_x(hu^2)+gh\partial_x(h+z_{\mathrm{b}})+\frac{1}{\rho}\frac{gh^2}{2}\partial_x\rho+\frac{1}{\rho}\partial_x(h\hat{p}_{\mathrm{nh}})&\\ =-2\frac{\hat{p}_{\mathrm{nh}}}{\rho}\partial_x z_{\mathrm{b}}-\tau+\left(1-\frac{\rho_0}{2\rho}\right)u\frac{E-D}{1-\psi_0},&\\ \partial_t(hw)+\partial_x(huw)=2\frac{\hat{p}_{\mathrm{nh}}}{\rho}+\left(1-\frac{\rho_0}{2\rho}\right)w\frac{E-D}{1-\psi_0}.&\end{aligned}$$

At this point, we make two assumptions to obtain a simplified model with a dissipative energy balance: firstly, we assume that the fluid and sediment densities are very close at the fluid/sediment interface. In fact, if the fluid density tends to the saturation density, then ρ may be approximated by ρ_0 in the transfer terms, which yields

$$1-\frac{\rho_0}{2\rho}\approx\frac{1}{2}.$$

Secondly, in the case of low concentrations, the Boussinesq assumption is justified. Then $\rho\approx\rho_{\mathrm{f}}$ in all terms except for the term representing the deviation from a hydrostatic pressure $\partial_x\rho$. Consequently, we obtain

$$\frac{1}{\rho}g\frac{h^2}{2}\partial_x\rho\approx\frac{1}{\rho_{\mathrm{f}}}g\frac{h^2}{2}\partial_x\rho=(r_{\mathrm{s}}-1)g\frac{h^2}{2}\partial_x c=(r_{\mathrm{s}}-1)\frac{g}{2}\left(h\partial_x(hc)-hc\partial_x h\right).$$

Therefore, the final simplified model reads

$$\begin{aligned}&\partial_t h+\partial_x(hu)=\frac{E-D}{1-\psi_0},\\ &\partial_t(hu)+\partial_x\left(hu^2+\frac{gh^2}{2}+hp_{\mathrm{nh}}\right)+(r_{\mathrm{s}}-1)\frac{g}{2}\left(h\partial_x(hc)-hc\,\partial_x h\right)\\ &\qquad\qquad=-(2p_{\mathrm{nh}}+gh)\partial_x z_{\mathrm{b}}-\frac{\hat{\tau}}{\rho_{\mathrm{f}}}+\frac{u}{2}\frac{E-D}{1-\psi_0},\\ &\partial_t(hw)+\partial_x(huw)=2p_{\mathrm{nh}}+\frac{w}{2}\frac{E-D}{1-\psi_0},\\ &\partial_t(hc)+\partial_x(huc)=E-D,\\ &\partial_t z_{\mathrm{b}}+\frac{1}{1-\psi_0}\partial_x q_{\mathrm{b}}=-\frac{E-D}{1-\psi_0},\\ &\partial_t h_{\mathrm{g}}=-(\dot{\eta}_{\mathrm{e}}-\dot{\eta}_{\mathrm{d}}),\end{aligned}\tag{2.7a}$$

together with the same incompressibility condition

$$w-u\partial_x z_{\mathrm{b}}+\partial_t z_{\mathrm{b}}+\frac{h}{2}\partial_x u=0.\tag{2.7b}$$

This model consists of seven partial differential equations from which one seeks to determine the same number of scalar unknowns, namely h, u, w, c, z_{b}, h_{g}, and p_{nh} as functions of horizontal spatial position x and time t.

2.2. **Bedload modelling.** The bedload discharge is typically determined based on the shear stress acting on the bed and the critical shear stress required to initiate sediment motion. When the shear stress exceeds the critical threshold, sediment transport occurs. Various empirical models exist to predict bedload discharge, but many exhibit limitations such as the absence of a dissipative energy balance, mass conservation inconsistencies, or restricted applicability to specific flow conditions

[16, 19]. In this subsection we present a class of bedload models that satisfies an energy balance (see Theorem 2). Firstly, non-equilibrium models are introduced. Secondly, the simplified case of equilibrium models, which is widely used in the literature, is presented. Finally, bedload models that take into account gravitational effects are discussed.

2.2.1. *Non-equilibrium bedload models.* In this case the bed evolution equations are given by

$$\partial_t z_{\mathrm{b}} + \frac{1}{1-\psi_0}\partial_x q_{\mathrm{b}} = -\frac{E-D}{1-\psi_0}, \quad \partial_t h_{\mathrm{g}} = \dot{\eta}_{\mathrm{d}} - \dot{\eta}_{\mathrm{e}},$$

where the bedload flux is modelled as $q_{\mathrm{b}} \coloneqq h_{\mathrm{m}} V_{\mathrm{b}}$, with $h_{\mathrm{m}} \coloneqq z_{\mathrm{b}} - h_{\mathrm{g}}$,

$$V_{\mathrm{b}} \coloneqq v_{\mathrm{b}} \sqrt{(r_{\mathrm{s}}-1) g d_{\mathrm{s}}},$$

and $r_{\mathrm{s}} = \rho_{\mathrm{s}}/\rho_{\mathrm{f}}$ the density ratio. The sediment transport velocity is given by

$$v_{\mathrm{b}} \coloneqq \mathrm{sgn}(\tau)(\sqrt{\theta} - \sqrt{\theta_{\mathrm{c}}})_+, \tag{2.8}$$

where the so-called Shields parameter θ is defined by

$$\theta \coloneqq \frac{|\tau|}{\rho_{\mathrm{f}}(r_{\mathrm{s}}-1) g d_{\mathrm{s}}},$$

and θ_{c} is the critical Shields parameter. Here τ represents the shear stress defined by

$$\frac{\tau}{\rho_{\mathrm{f}}} = C_{\mathrm{f}} u|u| \quad \text{with } C_{\mathrm{f}} = g n^2 h^{-1/3} \text{ (Manning law) or } C_{\mathrm{f}} = \xi/8 \text{ (Darcy-Weisbach law).} \tag{2.9}$$

Finally, the vertical entrainment and deposition rates are given by

$$\dot{\eta}_{\mathrm{e}} = (\theta - \theta_{\mathrm{c}})_+ \frac{k_{\mathrm{e}}}{1-\psi_0}\sqrt{(r_{\mathrm{s}}-1) g d_{\mathrm{s}}}, \quad \dot{\eta}_{\mathrm{d}} = h_{\mathrm{m}} \frac{k_{\mathrm{d}}}{d_{\mathrm{s}}}\sqrt{(r_{\mathrm{s}}-1) g d_{\mathrm{s}}}. \tag{2.10}$$

The erosion and deposition rates (E and D) are defined by empirical formulations, which will be detailed later in the numerical test (Section 4).

2.2.2. *Equilibrium bedload models.* If equilibrium conditions are assumed, i.e., $\dot{\eta}_{\mathrm{e}} = \dot{\eta}_{\mathrm{d}}$, we obtain by equating the right-hand sides in (2.10)

$$h_{\mathrm{m}} = \frac{d_{\mathrm{s}} k_{\mathrm{e}}}{k_{\mathrm{d}}(1-\psi_0)}(\theta - \theta_{\mathrm{c}})_+, \tag{2.11}$$

which leads to the simplified bedload flux

$$q_{\mathrm{b}} = \mathrm{sgn}(\tau)\frac{k_{\mathrm{e}}}{k_{\mathrm{d}}}(\theta - \theta_{\mathrm{c}})_+(\sqrt{\theta} - \sqrt{\theta_{\mathrm{c}}})\frac{d_{\mathrm{s}}}{1-\psi_0}\sqrt{(r_{\mathrm{s}}-1) g d_{\mathrm{s}}}. \tag{2.12}$$

This expression for q_{b} is substituted into the evolution equation for z_{b} in system (2.7a). Since the last equation, the evolution equation for h_{g}, is no longer needed, we obtain as a result the equilibrium version of model (2.7).

Notice that other definitions of $\dot{\eta}_{\mathrm{e}}$ and $\dot{\eta}_{\mathrm{d}}$ also imply different definitions of h_{m} for equilibrium models. The definition of h_{m} (2.11) implies the definition of q_{b} given by (2.12), that is a generalization of Ashida-Mishiue model [3]. Another variant of the definition of $\dot{\eta}_{\mathrm{e}}$ is

$$\dot{\eta}_{\mathrm{e}} = \frac{(\theta - \theta_{\mathrm{c}})_+^{3/2}}{\sqrt{\theta} - \sqrt{\theta_{\mathrm{c}}}}\frac{k_{\mathrm{e}}}{1-\psi_0}\sqrt{(r_{\mathrm{s}}-1) g d_{\mathrm{s}}},$$

which in the equilibrium case implies the solid transport discharge

$$q_{\mathrm{b}} = \mathrm{sgn}(\tau)\frac{k_{\mathrm{e}}}{k_{\mathrm{d}}}(\theta - \theta_{\mathrm{c}})_+^{3/2}\frac{d_{\mathrm{s}}}{1-\psi_0}\sqrt{(r_{\mathrm{s}}-1) g d_{\mathrm{s}}},$$

which is a generalization of the well-known Meyer-Peter and Müller model [27].

2.2.3. *Shear stress and gravitational effects.* The shear stress τ is typically chosen based on Manning's law but can be generalized to include gravitational effects in sediment transport. Following [19], we define an effective shear stress τ_{eff}:

$$\frac{\tau_{\text{eff}}}{\rho_{\text{f}}} = \frac{\tau}{\rho_{\text{f}}} - k_1 \partial_x (h + z_{\text{b}}) - k_2 \partial_x z_{\text{b}}, \tag{2.13}$$

where $k_1 \coloneqq \vartheta g d_{\text{s}}$, $k_2 \coloneqq \vartheta g d_{\text{s}}(r_{\text{s}} - 1)$, and $\vartheta \coloneqq \theta_{\text{c}} / \tan\delta$, with δ representing the angle of repose of the sediment material (commonly $\delta \approx 25°$). These additional terms account for gravitational effects through bed and free surface slopes. If τ_{eff} is used instead of τ then we obtain the effective Shields parameter

$$\theta_{\text{eff}} \coloneqq \frac{|\tau_{\text{eff}}|}{\rho_{\text{f}}(r_{\text{s}} - 1) g d_{\text{s}}}. \tag{2.14}$$

By writing τ_{eff} and θ_{eff} in place of τ and θ, respectively, in Eqs. (2.8) and (2.10) we obtain the final non-equilibrium model (2.7) with gravitational effects. Analogously, the final equilibrium model with gravitational effects is obtained by modifying Eq. (2.12) for the solid transport discharge accordingly with τ_{eff} and θ_{eff}.

If τ_{eff} as given by (2.13) is used within (2.14) , then equation (2.5) will include second-order spatial derivatives. Consequently, explicit numerical methods require a stability condition of CFL $\propto 1/\Delta x^2$, which leads to undesirably small time steps. To mitigate this issue, a semi-implicit method [19] should be employed to ensure numerical stability without excessively restricting the time step size. This is detailed in next section.

2.3. **Mass conservation.** The principle of mass conservation is essential for constructing accurate models of sediment transport. The sediment mass $m_{\text{s}} = m_{\text{s}}(x,t)$ and the fluid mass $m_{\text{f}} = m_{\text{f}}(x,t)$ at position x and time t are given by

$$\begin{aligned} m_{\text{s}}(x,t) &\coloneqq \rho_{\text{s}}\big(h(x,t)c(x,t) + (1-\psi_0) z_{\text{b}}(x,t)\big), \\ m_{\text{f}}(x,t) &\coloneqq \rho_{\text{f}}\big(h(x,t)(1-c(x,t)) + \psi_0 z_{\text{b}}(x,t)\big), \end{aligned}$$

respectively. Namely, we obtain the following result, which is obtained straightforward from (2.1), (2.4), and (2.5):

Theorem 1 (Mass conservation)**.** *The model satisfies mass conservation. Specifically, the model implies the equations of conservation of sediment and fluid mass*

$$\begin{aligned} \partial_t m_{\text{s}} + \partial_x \left(huc + q_{\text{b}}\right) &= 0, \\ \partial_t m_{\text{f}} + \partial_x \left(hu(1-c) + \frac{\psi_0}{1-\psi_0} q_{\text{b}}\right) &= 0. \end{aligned}$$

2.4. **Energy balance.** The solid transport discharge q_{b} is defined in Section 2.2 in several alternative forms. All these definitions can be written in the general form

$$q_{\text{b}} = h_{\text{m}} V_{\text{b}}, \quad V_{\text{b}} = u - P, \quad P \coloneqq C_1 \partial_x (h + z_{\text{b}}) + C_2 \partial_x z_{\text{b}} + C_3 (r_{\text{s}} - 1) \operatorname{sgn}(V_{\text{b}}) \tan\delta \tag{2.15}$$

with dimensional parameters C_1, C_2, C_3 that are defined in terms of physical values such as the gravity constant, the mean grain size diameter, and the critical Shields parameter (see Section 2.2). Moreover, $h_{\text{m}} = z_{\text{b}} - h_{\text{g}}$ for non-equilibrium models while h_{m} is defined by (2.11) for equilibrium models. Finally, we define

$$\hat{\tau} \coloneqq \tau + \rho_{\text{f}} h_{\text{m}} P, \tag{2.16}$$

where τ is a generic friction term (e.g., Manning or Darcy-Weisbach), see equation (2.9). This model satisfies the following dissipative energy balance:

Theorem 2 (Energy balance)**.** *Consider the system of equations (2.7), (2.15), and (2.16), describing shallow water flow with sediment transport and bed evolution. Then the total mechanical energy*

$$\mathcal{E} := \frac{g(h+z_\mathrm{b})^2}{2} + \frac{h(u^2+w^2)}{2}$$

satisfies the dissipative balance law:

$$\begin{aligned} &\partial_t \mathcal{E} + \partial_x \left(u \left(\frac{hu^2+hw^2}{2} + \frac{gh^2(1+c(r_\mathrm{s}-1))}{2} + p_\mathrm{nh} \right) + q_\mathrm{b}\, g(h+z_\mathrm{b}) + ghuz_\mathrm{b} \right) \\ &\leq -\left\{ (r_\mathrm{s}-1)h_\mathrm{m}|v_\mathrm{b}| \tan\delta + h_\mathrm{m}P^2 + u\,\frac{\tau}{\rho_\mathrm{f}} \right\} + c\partial_x(h^2u)\frac{g(r_\mathrm{s}-1)}{2}. \end{aligned} \tag{2.17}$$

For brevity we omit the proof, which is similar to the one presented in [16]. Clearly, term in curled brackets on the right-hand side of (2.17) is non-negative under standard physical assumptions, and hence it contributes to energy dissipation. However, the last term, which involves the spatial derivative $\partial_x(h^2u)$, is not in conservative form and, in principle, may act either as a source or a sink of energy depending on the sign of the derivative. However, the structure of the term allows for a meaningful interpretation. In regions where $\partial_x(h^2u) < 0$, the contribution is manifestly dissipative, since $c \in [0,1]$ and the entire term is non-positive. In regions where $\partial_x(h^2u) > 0$, the term can be rewritten as

$$c\partial_x(h^2u) = \partial_x(h^2u) - (1-c)\partial_x(h^2u),$$

where the first term $\partial_x(h^2u)$ is conservative and can be absorbed into the energy flux (especially under appropriate boundary conditions). The second term, $-(1-c)\partial_x(h^2u)$, is non-positive in this case and thus it contributes to dissipation. In general, we have the identity

$$c\,\partial_x(h^2u) = \partial_x\left(\frac{1+\mathrm{sgn}(\partial_x(h^2u))}{2}h^2u\right) - \left(\frac{1+\mathrm{sgn}(\partial_x(h^2u))}{2} - c\right)\partial_x(h^2u),$$

which is composed of a conservative term and a dissipative one. It follows that the full energy inequality consists of a collection of dissipative terms, and conservative fluxes that vanish under suitable boundary conditions. Therefore, the total mechanical energy satisfies a net dissipative balance law, and energy is non-increasing in time under these assumptions.

3. Numerical implementation

3.1. **Preliminaries.** To compute the model transition from time t_n to t_{n+1}, we should use a robust numerical scheme that can handle second derivatives, and preserve positivity of the needed variables. The discretization of governing system (2.7a) combines the following four ingredients: the underlying hydrostatic hyperbolic system with non-conservative products is solved; second-order derivative terms coming from the gravitational effects are included; source terms corresponding to the friction and erosion are deposition rates are incorporated; and non-hydrostatic pressure is computed and the horizontal and vertical velocities are accordingly corrected.

In the following we write the compact form of system (2.7a) in the non-equilibrium case but we do not include gravitational effects yet. These are handled in Section 3.5. To this aim, we denote by $\boldsymbol{W}$ the vector of conservative variables. The system (2.7a) is written in compact form as

$$\partial_t \boldsymbol{W} + \partial_x \boldsymbol{F}(\boldsymbol{W}) + \boldsymbol{B}(\boldsymbol{W})\partial_x \boldsymbol{W} = \boldsymbol{K}(\boldsymbol{W}) + \nabla_\mathrm{NH}\boldsymbol{Q},$$

where we define

$$\boldsymbol{W} \coloneqq \begin{pmatrix} h \\ hu \\ hw \\ hc \\ z_{\mathrm{b}} \\ h_{\mathrm{g}} \end{pmatrix}, \quad \boldsymbol{F}(\boldsymbol{W}) \coloneqq \begin{pmatrix} hu \\ hu^2 + gh^2/2 \\ huw \\ huc \\ q_{\mathrm{b}}/(1-\psi_0) \\ 0 \end{pmatrix}, \quad \boldsymbol{B}(\boldsymbol{W}) \coloneqq \begin{bmatrix} 0 & 0 & 0 & 0 & 0 & 0 \\ \gamma_h & 0 & 0 & \gamma_{hc} & gh & 0 \\ 0 & 0 & 0 & 0 & 0 & 0 \\ 0 & 0 & 0 & 0 & 0 & 0 \\ 0 & 0 & 0 & 0 & 0 & 0 \\ 0 & 0 & 0 & 0 & 0 & 0 \end{bmatrix}, \tag{3.1}$$

along with $\gamma_h \coloneqq -(g/2)(r_{\mathrm{s}}-1)hc$, $\gamma_{hc} \coloneqq (g/2)(r_{\mathrm{s}}-1)h$, and the source and non-hydrostatic terms

$$\boldsymbol{K}(\boldsymbol{W}) \coloneqq \begin{pmatrix} 0 \\ -\tau \\ 0 \\ 0 \\ 0 \\ \dot{\eta}_{\mathrm{d}} - \dot{\eta}_{\mathrm{e}} \end{pmatrix} + \frac{E-D}{1-\psi_0} \begin{pmatrix} 1 \\ u/2 \\ w/2 \\ 1-\psi_0 \\ -1 \\ 0 \end{pmatrix}, \quad \nabla_{\mathrm{NH}} \boldsymbol{Q} = \begin{pmatrix} 0 \\ -\partial_x(hq) - 2q\partial_x z_{\mathrm{b}} \\ 2q \\ 0 \\ 0 \\ 0 \end{pmatrix}.$$

We now describe the steps of the numerical scheme for non-equilibrium model with gravitational effects and non-hydrostatic pressure. This scheme is easily adapted to particular cases as hydrostatic pressure, the absence of gravitational effects, or the equilibrium regime. For simplicity, at each step we assume that the solution evolves from time t_* to t_{n+1}. So, $\boldsymbol{W}^*$ must be understood as the output of a previous stage.

3.2. **Finite volume method for hyperbolic system with non-conservative products.** We adopt the path-conservative framework [12, 28, 29] to deal with possible discontinuities in the solutions and the presence of non-conservative products in the underlying hyperbolic part of the system, i. e.,

$$\partial_t \boldsymbol{W} + \partial_x \boldsymbol{F}(\boldsymbol{W}) + \boldsymbol{B}(\boldsymbol{W})\partial_x \boldsymbol{W} = \boldsymbol{0}. \tag{3.2}$$

This system can be written in quasi-linear form as $\partial_t \boldsymbol{W} + \boldsymbol{A}(\boldsymbol{W})\partial_x \boldsymbol{W} = \boldsymbol{0}$ with the 6×6 matrix $\boldsymbol{A}(\boldsymbol{W}) \coloneqq \partial \boldsymbol{F}(\boldsymbol{W})/\partial \boldsymbol{W} + \boldsymbol{B}(\boldsymbol{W})$, whose eigenvalues are $\lambda \in \{0, u\}$ plus the four eigenvalues of the reduced matrix

$$\hat{\boldsymbol{A}}(\boldsymbol{W}) \coloneqq \begin{bmatrix} 0 & 1 & 0 & 0 \\ -u^2 + gh + \gamma_h & 2u & \gamma_{hc} & gh \\ -uc & c & u & 0 \\ \alpha_h & \alpha_{hu} & 0 & \alpha_{z_{\mathrm{b}}} \end{bmatrix}, \quad \alpha_\xi \coloneqq \frac{1}{1-\psi_0}\partial_\xi q_{\mathrm{b}} \quad \text{for } \xi \in \{h, hu, z_{\mathrm{b}}\}.$$

In practice only very small values of concentration c are assumed, and the contribution of c just for the computation of eigenvalues is neglected. Consequently, if we assume $c \ll 1$ in $\hat{\boldsymbol{A}}$, then the eigenvalues of $\boldsymbol{A}(\boldsymbol{W})$ are 0, u, and u, and the eigenvalues of

$$\tilde{\boldsymbol{A}}(\boldsymbol{W}) \coloneqq \begin{bmatrix} 0 & 1 & 0 \\ -u^2 + gh + \gamma_h & 2u & gh \\ \alpha_h & \alpha_{hu} & \alpha_{z_{\mathrm{b}}} \end{bmatrix}. \tag{3.3}$$

The FV discretization is based on the subdivision of the horizontal domain into uniform control volumes $V_i \coloneqq [x_{i-1/2}, x_{i+1/2}]$ of length Δx for $i \in \mathcal{I}$. It is assumed that $\boldsymbol{W}_i^n$ approximates the cell average of $\boldsymbol{W}$ on V_i at time t_n, i.e.,

$$\boldsymbol{W}_i^n \coloneqq \frac{1}{\Delta x} \int_{V_i} \boldsymbol{W}(x, t_n)\, \mathrm{d}x.$$

For convenience, in the discretization we separate the convective and pressure terms in $\boldsymbol{F}(\boldsymbol{W})$. To this end we replace (3.2) by

$$\partial_t \boldsymbol{W} + \partial_x \boldsymbol{F}_{\mathrm{c}}(\boldsymbol{W}) + \boldsymbol{S}(\boldsymbol{W})\partial_x(h + z_{\mathrm{b}}) + \tilde{\boldsymbol{B}}(\boldsymbol{W})\partial_x \boldsymbol{W} = \boldsymbol{0},$$

where we define $\boldsymbol{S}(\boldsymbol{W}) \coloneqq (0, gh, 0, 0, 0, 0)^{\mathrm{T}}$. A usual first-order path-conservative explicit scheme now reads

$$\boldsymbol{W}_i^{n+1} = \boldsymbol{W}_i^n - \frac{\Delta x}{\Delta t}\left(\boldsymbol{\mathcal{F}}_{i+1/2}^n - \boldsymbol{\mathcal{F}}_{i-1/2}^n + \frac{1}{2}\big(\tilde{\boldsymbol{\mathcal{B}}}_{i+1/2}^n + \tilde{\boldsymbol{\mathcal{B}}}_{i-1/2}^n + \boldsymbol{\mathcal{S}}_{i+1/2}^n + \boldsymbol{\mathcal{S}}_{i-1/2}^n\big)\right),$$

where we define

$$\begin{aligned}
\tilde{\boldsymbol{\mathcal{B}}}_{i+1/2}^n &\coloneqq \frac{1}{2}\big(\tilde{\boldsymbol{B}}(\boldsymbol{W}_i^n) + \tilde{\boldsymbol{B}}(\boldsymbol{W}_{i+1}^n)\big)\big(\boldsymbol{W}_{i+1}^n - \boldsymbol{W}_i^n\big) \quad \text{and} \\
\boldsymbol{\mathcal{S}}_{i+1/2}^n &\coloneqq \frac{1}{2}\big(\boldsymbol{S}(\boldsymbol{W}_i^n) + \boldsymbol{S}(\boldsymbol{W}_{i+1}^n)\big)\big(h_{i+1/2}^{n,+} - h_{i+1/2}^{n,-}\big),
\end{aligned}$$

where $h_{i+1/2}^{n,\pm}$ are the reconstructed states to approximate the free surface gradient given by

$$\begin{aligned}
h_{i+1/2}^{n,+} &\coloneqq \max\big\{h_{i+1}^n + z_{\mathrm{b},i+1}^n - z_{i+1/2}^{*,n}, 0\big\}, \\
h_{i+1/2}^{n,-} &\coloneqq \max\big\{h_i^n + z_{\mathrm{b},i}^n - z_{i+1/2}^{*,n}, 0\big\}, \quad \text{and} \\
z_{i+1/2}^{*,n} &\coloneqq \max\big\{z_{\mathrm{b},i}^n, z_{\mathrm{b},i+1}^n\big\}.
\end{aligned}$$

These states are also useful to handle wet/dry areas. In what follows we omit the upper index n for simplicity. The numerical flux $\boldsymbol{\mathcal{F}}_{i+1/2}$ is defined according to a PVM scheme (see [11]), where the viscosity matrix is defined as a polynomial evaluation of the Roe matrix $\boldsymbol{A}_{i+1/2}$. This matrix is assumed to satisfy the relation

$$\boldsymbol{A}_{i+1/2}(\boldsymbol{W}_{i+1} - \boldsymbol{W}_i) = \boldsymbol{F}(\boldsymbol{W}_{i+1}) - \boldsymbol{F}(\boldsymbol{W}_i) + \int_0^1 \boldsymbol{B}_\Phi(s; \boldsymbol{W}_{i+1}, \boldsymbol{W}_i)\partial_s \Phi(s; \boldsymbol{W}_{i+1}, \boldsymbol{W}_i)\,\mathrm{d}s,$$

where $\boldsymbol{F}$ and $\boldsymbol{B}$ are as given in (3.1). For convenience, we assume a general second-order PVM scheme. This includes all particular cases studied herein, namely the Rusanov, HLL, and PVM-2I schemes. Then the general numerical flux is

$$\begin{aligned}
\boldsymbol{\mathcal{F}}_{i+1/2} = \frac{1}{2}\big(\boldsymbol{F}_{\mathrm{c}}(\boldsymbol{W}_{i+1}) + \boldsymbol{F}_{\mathrm{c}}(\boldsymbol{W}_i)\big) - \frac{1}{2}\Big(&\alpha_{0,i+1/2}\big(\boldsymbol{W}_{i+1/2}^+ - \boldsymbol{W}_{i+1/2}^-\big) \\
&+ (\alpha_{1,i+1/2}\boldsymbol{I} + \alpha_{2,i+1/2}\boldsymbol{A}_{i+1/2})\big(\boldsymbol{F}(\boldsymbol{W}_{i+1}) - \boldsymbol{F}(\boldsymbol{W}_i) + \tilde{\boldsymbol{\mathcal{B}}}_{i+1/2} + \boldsymbol{\mathcal{S}}_{i+1/2}\big)\Big)
\end{aligned} \tag{3.4}$$

with $\boldsymbol{I}$ the identity matrix, and $\boldsymbol{W}_{i+1/2}^{\pm}$ are the reconstructed states

$$\begin{aligned}
\boldsymbol{W}_{i+1/2}^- &\coloneqq \big(h_{i+1/2}^-, h_{i+1/2}^- u_i, h_{i+1/2}^- w_i, h_{i+1/2}^- c_i, z_{\mathrm{b},i}, h_{\mathrm{g},i}\big)^{\mathrm{T}}, \\
\boldsymbol{W}_{i+1/2}^+ &\coloneqq \big(h_{i+1/2}^+, h_{i+1/2}^+ u_{i+1}, h_{i+1/2}^+ w_{i+1}, h_{i+1/2}^+ c_{i+1}, z_{\mathrm{b},i+1}, h_{\mathrm{g},i+1}\big)^{\mathrm{T}}.
\end{aligned}$$

Notice that the reconstructed states are used just for the well-balancing of the scheme and the wet/dry treatment.

3.3. **Well-balanced property of HLL and Rusanov methods for SVE systems.** The well-balance property of the scheme is a requirement not only to preserve steady solutions but also to reproduce solutions that consist in small perturbations (similar to the truncation error of the method) of equilibrium states. For the design of the scheme for (2.7a) we focus on equilibrium

states at rest, although other equilibrium states with $u \neq 0$ will equally be preserved (see, e.g., Section 4.2). The steady states at rest (with no erosion) satisfy

$$h + z_{\mathrm{b}} = \text{constant}, \quad |\partial_x z_{\mathrm{b}}| < \tan\delta, \quad u = w = p_{\mathrm{nh}} = 0, \quad c = 0, \quad E = D, \quad \dot{\eta}_{\mathrm{e}} = \dot{\eta}_{\mathrm{d}}. \tag{3.5}$$

The condition for the bottom slope is deduced from $\theta_{\mathrm{eff}} < \theta_{\mathrm{c}}$ with $u = 0$ and $h + z_{\mathrm{b}} = \text{const}$. It is remarkable that these are steady states when gravitational effects are incorporated. Otherwise, no condition on the bottom slope is necessary.

The Rusanov and HLL methods are defined by (3.4) where the numerical diffusion of the scheme is defined in terms of the constant and first-order polynomials $P_0^{\mathrm{RU}}(x)$ and $P_1^{\mathrm{HLL}}(x)$, respectively, given by $\alpha_2^{\mathrm{RU}} = \alpha_2^{\mathrm{HLL}} = 0$ and

$$\begin{aligned} &P_0^{\mathrm{RU}}(x) \coloneqq \alpha_0^{\mathrm{RU}} \quad \text{with } \alpha_0^{\mathrm{RU}} \coloneqq \max(\{|S_{\mathrm{L}}|, |S_{\mathrm{R}}|\}, \\ &P_1^{\mathrm{HLL}}(x) \coloneqq \alpha_0^{\mathrm{HLL}} + \alpha_1^{\mathrm{HLL}} x \quad \text{with} \quad \alpha_0^{\mathrm{HLL}} \coloneqq \frac{S_{\mathrm{R}}|S_{\mathrm{L}}| - S_{\mathrm{L}}|S_{\mathrm{R}}|}{S_{\mathrm{R}} - S_{\mathrm{L}}}, \quad \alpha_1^{\mathrm{HLL}} \coloneqq \frac{|S_{\mathrm{R}}| - |S_{\mathrm{L}}|}{S_{\mathrm{R}} - S_{\mathrm{L}}}, \end{aligned} \tag{3.6}$$

where S_{L} and S_{R} are approximations of the largest and the smallest eigenvalues, respectively, of the Roe matrix of the system $\boldsymbol{A}_{i+1/2}$.

These definitions do not lead to a well-balanced scheme in the case of an SVE system due to the evolution equation for the sediment layer z_{b}. Concretely, the term $\alpha_{0,i+1/2}(z_{\mathrm{b},i+1} - z_{\mathrm{b},i})$ does not vanish in that equation for steady states. This behaviour results in a non-physical erosion of the bed. In [22] a modification of HLL method was proposed that neglects this term (in combination with an upwind approximation). Apart from that, to the best of our knowledge from literature, well-balanced Rusanov or HLL-type schemes for sediment transport problems have not been developed so far. Here we propose a simple modification of the Rusanov and HLL schemes for system (2.7a) with the well-balance property. This modification consists of an appropriate correction to the numerical viscosity related to the contribution $\alpha_{0,i+1/2}(z_{\mathrm{b},i+1} - z_{\mathrm{b},i})$ inspired by the case of the equilibrium model. So, a compelling approach to address this problem involves interpreting the non-equilibrium model as a generalization of the SVE framework. To this end, we consider the evolution equations for the bottom layer variables z_{b}, h_{m} and h_{g}:

$$\partial_t z_{\mathrm{b}} + \frac{1}{1-\psi_0}\partial_x q_{\mathrm{b}} = 0, \qquad \partial_t h_{\mathrm{m}} + \frac{1}{1-\psi_0}\partial_x q_{\mathrm{b}} = 0, \qquad \partial_t h_{\mathrm{g}} = 0,$$

where for sake of simplicity, we neglect erosion or deposition contributions (i.e., we set $E = D$) as in the steady state (3.5). In general, we use the equations for z_{b} and h_{g} to compute h_{m} as $z_{\mathrm{b}} - h_{\mathrm{g}}$. Let us consider the Rusanov or HLL method to evolve from t_n to t_{n+1}, i.e.,

$$\begin{aligned} z_{\mathrm{b},i}^{n+1} = z_{\mathrm{b},i}^n &- \frac{\Delta t}{\Delta x}\left(\frac{q_{\mathrm{b},i}^n + q_{\mathrm{b},i+1}^n}{2} - \frac{1}{2}\left(\alpha_{0,i+1/2}^n \Delta z_{\mathrm{b},i+1/2}^n + \alpha_{1,i+1/2}^n \Delta q_{\mathrm{b},i+1/2}^n\right)\right) \\ &+ \frac{\Delta t}{\Delta x}\left(\frac{q_{\mathrm{b},i}^n + q_{\mathrm{b},i-1}^n}{2} - \frac{1}{2}\left(\alpha_{0,i-1/2}^n \Delta z_{\mathrm{b},i-1/2}^n + \alpha_{1,i-1/2}^n \Delta q_{\mathrm{b},i-1/2}^n\right)\right), \end{aligned} \tag{3.7a}$$

$$\begin{aligned} h_{\mathrm{m},i}^{n+1} = h_{\mathrm{m},i}^n &- \frac{\Delta t}{\Delta x}\left(\frac{q_{\mathrm{b},i}^n + q_{\mathrm{b},i+1}^n}{2} - \frac{1}{2}\left(\alpha_{0,i+1/2}^n \Delta h_{\mathrm{m},i+1/2}^n + \alpha_{1,i+1/2}^n \Delta q_{\mathrm{b},i+1/2}^n\right)\right) \\ &+ \frac{\Delta t}{\Delta x}\left(\frac{q_{\mathrm{b},i}^n + q_{\mathrm{b},i-1}^n}{2} - \frac{1}{2}\left(\alpha_{0,i-1/2}^n \Delta h_{\mathrm{m},i-1/2}^n + \alpha_{1,i-1/2}^n \Delta q_{\mathrm{b},i-1/2}^n\right)\right), \end{aligned} \tag{3.7b}$$

$$h_{\mathrm{g},i}^{n+1} = h_{\mathrm{g},i}^n, \tag{3.7c}$$

where α_0, α_1 are defined by (3.6), and $\Delta\xi_{i+1/2} = \xi_{i+1} - \xi_i$ for $\xi \in \{z_\mathrm{b}, h_\mathrm{m}, q_\mathrm{b}\}$. By subtracting (3.7b) from (3.7a) we obtain for h_g

$$h_{\mathrm{g},i}^{n+1} - h_{\mathrm{g},i}^{n} = \frac{1}{2}\frac{\Delta t}{\Delta x}\left[\alpha_{0,i+1/2}^{n}\left(\Delta z_{\mathrm{b},i+1/2}^{n} - \Delta h_{\mathrm{m},i+1/2}^{n}\right) - \alpha_{0,i-1/2}^{n}\left(\Delta z_{\mathrm{b},i-1/2}^{n} - \Delta h_{\mathrm{m},i-1/2}^{n}\right)\right],$$

whose right-hand side term will not vanish in general. This property produces an inconsistency error with respect to (3.7c) due to the numerical diffusion.

This inconsistency may lead to different numerical results depending on the pair of equations used to compute z_b, h_m, and h_g. In some cases, it may even produce unphysical values such as negative h_m (or z_b, h_g, depending on the formulation), or more generally, violate the relation $z_\mathrm{b} = h_\mathrm{m} + h_\mathrm{g}$ at the discrete level. Therefore, it is necessary to introduce a modified approach that resolves the discrepancy in the numerical viscosity term while ensuring consistency with the stationary solutions. To handle this issue we propose to replace the discrete differences Δz_b and Δh_m in Eqs. (3.7a) and (3.7b), respectively, by a consistent approximation based on the equilibrium model:

$$h_\mathrm{m}^{\mathrm{eq}} = \frac{d_\mathrm{s} k_\mathrm{e}}{(1-\psi_0)k_\mathrm{d}}(\theta - \theta_\mathrm{c})_+,$$

However, since Δz_b originally appears in the numerical viscosity term, it plays a crucial role in determining the direction of artificial diffusion. In fact, replacing Δz_b by $\Delta h_\mathrm{m}^{\mathrm{eq}}$ without adjusting its sign may lead to inconsistencies in the numerical flux. To address this issue, we replace the expression of the discrete jump $\Delta z_{\mathrm{b},i+1/2}$ and $\Delta h_{\mathrm{m},i+1/2}$ in (3.7a) and (3.7b) by

$$\Delta h_{\mathrm{m},i+1/2}^{\mathrm{eq}} = \frac{d_\mathrm{s} k_\mathrm{e}}{(1-\psi_0)k_\mathrm{d}}\left|(\theta_{i+1} - \theta_\mathrm{c})_+ - (\theta_i - \theta_\mathrm{c})_+\right| \mathrm{sgn}(\Delta z_{\mathrm{b},i+1/2}),$$

where we explicitly include the sign of the slope. This formulation ensures that we use the appropriate sign to preserve the directionality of the numerical viscosity. Thus, artificial oscillations or inconsistencies in the discrete sediment flux are avoided. Moreover, this modification guarantees consistency in the computation of z_b, h_m, and h_g independently of the chosen pair of equations in (3.7). It also preserves the desired steady states when $\theta_\mathrm{eff} < \theta_\mathrm{c}$, since $h_{\mathrm{m},i+1/2}^{\mathrm{eq}}$ naturally vanishes in those regions. Finally, since this correction is consistent with the definition of the equilibrium model, it results in a well-balanced scheme also in the equilibrium case.

3.4. **PVM-2I method.** The introduction of a new accurate scheme for sediment transport is motivated by some shortcomings of the Rusanov and HLL methods. They are not only not well-balanced (without corrections) as mentioned earlier, but also introduce a high level of numerical viscosity, especially for the evolution equation of z_b, which causes excessively rapid, physically inaccurate erosion. To handle these issues we propose a combination of the Rusanov or HLL method with a three-wave PVM method. The resulting new method will be denoted as PVM-2I method (since it is defined by a quadratic polynomial and employs an intermediate eigenvalue), and it is well-balanced by construction. The main idea is, in order to reduce the numerical diffusion associated to the bottom evolution equation, to use a second-degree PVM method just for that equation. Thus, the PVM-2I method is defined by the numerical flux (3.4) for all unknowns except for the sediment bed, that in this case is

$$\begin{aligned}[\boldsymbol{\mathcal{F}}_{i+1/2}]_{z_\mathrm{b}} = {} & \frac{1}{2}(q_{\mathrm{b},i} + q_{\mathrm{b},i+1}) \\ & - \frac{1}{2}\big(\alpha_{0,i+1/2}^{\mathrm{2I}}\Delta z_{\mathrm{b},i+1/2} + \alpha_{1,i+1/2}^{\mathrm{2I}}\Delta q_{\mathrm{b},i+1/2} + \alpha_{2,i+1/2}^{\mathrm{2I}}[\boldsymbol{A}_{i+1/2}\Delta\boldsymbol{F}_{i+1/2}]_{z_\mathrm{b}}\big),\end{aligned} \tag{3.8}$$

where $[\boldsymbol{A}_{i+1/2}\Delta\boldsymbol{F}_{i+1/2}]_{z_\mathrm{b}}$ denotes the component corresponding to the evolution of z_b of the product

$$\boldsymbol{A}_{i+1/2}\Delta\boldsymbol{F}_{i+1/2} = \boldsymbol{A}_{i+1/2}\big(\boldsymbol{F}(\boldsymbol{W}_{i+1}) - \boldsymbol{F}(\boldsymbol{W}_i) + \tilde{\boldsymbol{\mathcal{B}}}_{i+1/2} + \boldsymbol{\mathcal{S}}_{i+1/2}\big),$$

and $\alpha^{2\mathrm{I}}_{k,i+1/2}$, $k = 0, 1, 2$, are the coefficients of the polynomial $P_2^{2\mathrm{I}}(x) \coloneqq \alpha_0^{2\mathrm{I}} + \alpha_1^{2\mathrm{I}}x + \alpha_2^{2\mathrm{I}}x^2$ that satisfies $P_2(S_\mathrm{L}) = |S_\mathrm{L}|$, $P_2(S_\mathrm{I}) = |S_\mathrm{I}|$, and $P_2(S_\mathrm{R}) = |S_\mathrm{R}|$, where S_I is an estimate of an intermediate eigenvalue, which is detailed below. The coefficients of this polynomial are given by

$$\begin{aligned} &\alpha_0^{2\mathrm{I}} = \alpha_0^{\mathrm{HLL}} + \alpha_2^{2\mathrm{I}} S_\mathrm{L} S_\mathrm{R}, \quad \alpha_1^{2\mathrm{I}} = \alpha_1^{\mathrm{HLL}} - \alpha_2^{2\mathrm{I}}(S_\mathrm{R} + S_\mathrm{L}), \\ &\alpha_2^{2\mathrm{I}} = \frac{(|S_\mathrm{R}| - |S_\mathrm{I}|)(S_\mathrm{I} - S_\mathrm{L}) - (|S_\mathrm{I}| - |S_\mathrm{L}|)(S_\mathrm{R} - S_\mathrm{I})}{(S_\mathrm{R} - S_\mathrm{L})(S_\mathrm{R} - S_\mathrm{I})(S_\mathrm{I} - S_\mathrm{L})}. \end{aligned} \tag{3.9}$$

The key point is that S_I is chosen in such a way that $S_\mathrm{I} = 0$ in the case of no sediment transport. So, $\alpha_0^{2\mathrm{I}} = 0$ in such case, and the diffusion term in (3.8) vanishes, therefore steady solutions are preserved and non-physical erosion is avoided. With this in mind, we choose S_I as the intermediate eigenvalue of the simplified Roe matrix $\tilde{\boldsymbol{\mathcal{A}}}_{i+1/2}$ given by (3.3). Notice that the new coefficients (3.9) can be seen as a correction of the numerical viscosity associated to the usual HLL scheme.

Let us remark that the PVM-2I scheme preserves the positivity of the water depth since it coincides with HLL for the mass and momentum equations for these equations (see [5]). It is worth mentioning that we are not able to prove the water depth positivity when applying the second-degree PVM with $\alpha^{2\mathrm{I}}_{0,1,2}$ given by (3.9) for the whole system. Furthermore, although we do not have a general proof of positivity of the sediment bed for the PVM-2I scheme, we have not observed related troubles in the numerical experiments. Actually, positivity can be controlled by diminishing the time step, and the bed evolution is related to a much smaller velocity than water waves. Consequently, as long as the time step is adapted with a CFL condition suitable for water waves, it is sufficiently small to handle the bed evolution. This property explains why in practice we have not found any trouble with sediment positivity thickness.

3.5. **Semi-implicit step for gravitational terms.** In numerical modelling of sediment transport, gravitational terms influence the vertical motion of particles, particularly their settling and redistribution. A fully explicit approach to incorporate gravitational effects may impose restrictive time-step constraints due to stability limitations, particularly when dealing with fine sediment or high particle concentrations. To overcome these limitations, a semi-implicit numerical scheme is employed, which enhances stability while maintaining computational efficiency. The semi-implicit formulation discretizes the gravitational terms in a manner that allows for larger time steps without introducing significant numerical errors. By treating some components implicitly, the method mitigates the instability associated with rapid particle settling while preserving accuracy.

First, following [19], rewrite the solid transport discharge in a form that is convenient for its discretization. Then, using the interpretation $\operatorname{sgn}(\tau_\mathrm{eff}) = \tau_\mathrm{eff}/|\tau_\mathrm{eff}|$, we may rewrite the solid transport discharge term as

$$\frac{1}{1-\psi_0} q_\mathrm{b} = \tilde{q}_\mathrm{b}\tau_\mathrm{eff} = \tilde{q}_\mathrm{b}\big(C_\mathrm{f} u|u| - \partial_x(k_1(h + z_\mathrm{b}) + k_2 z_\mathrm{b})\big),$$

with $k_1 \coloneqq \vartheta g d_\mathrm{s}$, $k_2 \coloneqq \vartheta g d_\mathrm{s}(r_\mathrm{s} - 1)$, $\vartheta \coloneqq \theta_\mathrm{c}/\tan\delta$, and

$$\tilde{q}_\mathrm{b} = \frac{h_\mathrm{m}\sqrt{(r_\mathrm{s}-1)g d_\mathrm{s}}\,(\sqrt{\theta_\mathrm{eff}} - \sqrt{\theta_\mathrm{c}})_+}{(1-\psi_0)|\tau_\mathrm{eff}/\rho_\mathrm{f}|}.$$

At this point, we incorporate the gravitational effects for the sediment evolution equation (z_b), which is discretized in time as

$$z_\mathrm{b}^{n+1} = z_\mathrm{b}^n - \Delta t\partial_x\left(\tilde{q}_\mathrm{b}^n(C_\mathrm{f}^n u^n|u^n| - k_1\partial_x(h^{n+1} + z_\mathrm{b}^{n+1}) - k_2\partial_x z_\mathrm{b}^{n+1})\right).$$

Using the $\Theta-$method, we get

$$z_{\mathrm{b}}^{n+1} = z_{\mathrm{b}}^{n} - \Delta t \partial_x(\tilde{q}_{\mathrm{b}}^{n} C_{\mathrm{f}}^{n} u^{n}|u^{n}|) + (1-\Theta)\Delta t \partial_x \left(\tilde{q}_{\mathrm{b}}^{n}(k_1 \partial_x(h^{n} + z_{\mathrm{b}}^{n}) + k_2 \partial_x z_{\mathrm{b}}^{n})\right) + \Theta \Delta t \partial_x \left(\tilde{q}_{\mathrm{b}}^{n}(k_1 \partial_x(h^{n+1} + z_{\mathrm{b}}^{n+1}) + k_2 \partial_x z_{\mathrm{b}}^{n+1})\right),$$

where h^{n+1} was computed in the first hyperbolic step, see section 3.2. After using finite difference approximations for the space derivatives, a tridiagonal linear system for the unknowns $z_{\mathrm{b},i}^{n+1}$ is solved.

We remark that, in case of dealing with subcritical flows ($\mathrm{Fr} \ll 1$) a semi-implicit discretization as in [19], where the pressure gradient is removed from the stability restriction, may be convenient to improve the efficiency of large-time simulations. However, this is not the goal of this paper and it has not been implemented here.

3.6. **Source terms related to erosion and deposition.** In this step, we add the source terms related with the erosion (E/D) and deposition velocities ($\dot{\eta}_{\mathrm{e}}/\dot{\eta}_{\mathrm{d}}$). In order to ensure the positivity of the variables z_{b}, h_{g}, h_{m}, and c we define

$$\hat{E} := \frac{E^{n}(h_{\mathrm{m}}^{n+1} + h_{\mathrm{g}}^{n+1})}{h_{\mathrm{m}}^{n} + h_{\mathrm{g}}^{n}} \qquad \text{and} \qquad \hat{D} := \frac{(hc)^{n+1} D^{n}}{(hc)^{n}},$$

and apply a semi-implicit treatment similar to that of [21]. At each control volume V_i, this yields

$$\begin{aligned}
(1-\psi_0)h_{\mathrm{m}}^{n+1} &= (1-\psi_0)h_{\mathrm{m}}^{*} + (1-\psi_0)\Delta t\left(h_{\mathrm{g}}^{n+1}\frac{\dot{\eta}_{\mathrm{e}}^{n}}{h_{\mathrm{g}}^{n}} - h_{\mathrm{m}}^{n+1}\frac{\dot{\eta}_{\mathrm{d}}^{n}}{h_{\mathrm{m}}^{n}}\right) - \Delta t(\hat{E}-\hat{D}),\\
(1-\psi_0)h_{\mathrm{g}}^{n+1} &= (1-\psi_0)h_{\mathrm{g}}^{*} - (1-\psi_0)\Delta t\left(h_{\mathrm{g}}^{n+1}\frac{\dot{\eta}_{\mathrm{e}}^{n}}{h_{\mathrm{g}}^{n}} - h_{\mathrm{m}}^{n+1}\frac{\dot{\eta}_{\mathrm{d}}^{n}}{h_{\mathrm{m}}^{n}}\right),\\
(hc)^{n+1} &= (hc)^{*} + \Delta t(\hat{E}-\hat{D}),
\end{aligned} \tag{3.10}$$

where for sake of simplicity the spatial index i was omitted. The linear system (3.10) is solved for h_{m}^{n+1}, h_{g}^{n+1}, and $(hc)^{n+1}$. Next, we update the height and discharges as

$$\begin{aligned}
h^{n+1} &= h^{*} + \frac{\Delta t}{1-\psi_0}(\hat{E}-\hat{D}),\\
(hu)^{n+1} &= (hu)^{*} + \frac{u^{n}}{2}\frac{\Delta t}{1-\psi_0}(\hat{E}-\hat{D}) - \Delta t C_{\mathrm{f}}^{n}|u^{n}|u^{n+1},\\
(hw)^{n+1} &= (hw)^{*} + \frac{w^{n}}{2}\frac{\Delta t}{1-\psi_0}(\hat{E}-\hat{D}).
\end{aligned}$$

Notice that the use of $\hat{E}$ and $\hat{D}$ instead of E and D, respectively, in the previous equations guarantees that $\partial_t(h+z_{\mathrm{b}}) + \partial_x(hu + q_{\mathrm{b}}/(1-\psi_0)) = 0$ holds also at discrete level. The following theorem ensures the positivity of h_{g}, z_{b} and hc. Moreover, the positivity of h_{m} is ensured under an additional condition. We have verified the positivity of h_{m} in all simulations, even if this property has not been proven analytically.

Theorem 3 (Positivity of the variables)**.** *Assume that $h_{\mathrm{m}}^{*} \geq 0$, $h_{\mathrm{g}}^{*} \geq 0$, and $(hc)^{*} \geq 0$ are given, and that h_{m}^{n+1}, h_{g}^{n+1}, and $(hc)^{n+1}$, are to be determined from the linear system of equations (3.10). Then the system has a unique solution with the following properties:*

i) $z_{\mathrm{b}}^{n+1} := h_{\mathrm{m}}^{n+1} + h_{\mathrm{g}}^{n+1} \geq 0$, $h_{\mathrm{g}}^{n+1} \geq 0$, *and* $(hc)^{n+1} \geq 0$.

ii) A sufficient (but not necessary) condition to ensure $h_{\mathrm{m}}^{n+1} \geq 0$ *is*

$$E^n \leq \dot{\eta}_e^n (1-\psi_0) \frac{z_{\mathrm{b}}^n}{h_{\mathrm{g}}^n}. \tag{3.11}$$

Proof. For sake of clarity, we introduce $x_0 \coloneqq (1-\psi_0)h_{\mathrm{m}}^*$, $y_0 \coloneqq (1-\psi_0)h_{\mathrm{g}}^*$, $w_0 \coloneqq (hc)^*$, and

$$a = \Delta t \frac{\dot{\eta}_{\mathrm{e}}^n}{h_{\mathrm{g}}^n}, \quad b = \Delta t \frac{\dot{\eta}_{\mathrm{d}}^n}{h_{\mathrm{m}}^n}, \quad e = \frac{\Delta t}{1-\psi_0} \frac{E^n}{h_{\mathrm{m}}^n + h_{\mathrm{g}}^n}, \quad f = \Delta t \frac{D^n}{(hc)^n};$$

then the system (3.10) can be written as

$$\begin{bmatrix} 1+b+e & e-a & -f \\ -b & 1+a & 0 \\ -e & -e & 1+f \end{bmatrix} \begin{pmatrix} (1-\psi_0)h_{\mathrm{m}}^{n+1} \\ (1-\psi_0)h_{\mathrm{g}}^{n+1} \\ (hc)^{n+1} \end{pmatrix} = \begin{pmatrix} x_0 \\ y_0 \\ w_0 \end{pmatrix}.$$

The solution of this system is

$$\begin{aligned}
(1-\psi_0)h_{\mathrm{m}}^{n+1} &= \frac{(1+a+f)x_0 + af(x_0+y_0+w_0) + (a-e)y_0 + fw_0}{(1+a+b)(1+e+f)}, \\
(1-\psi_0)h_{\mathrm{g}}^{n+1} &= \frac{(1+b+e+f)y_0 + bf(x_0+y_0+w_0) + bx_0}{(1+a+b)(1+e+f)}, \\
(hc)^{n+1} &= \frac{w_0 + e(x_0+y_0+w_0)}{1+e+f}.
\end{aligned}$$

Since the coefficients a, b, e, and f are non-negative, and since we assume that $h_{\mathrm{m}}^* \geq 0$, $h_{\mathrm{g}}^* \geq 0$ and $(hc)^* \geq 0$, it follows that $x_0, y_0, w_0 \geq 0$, hence $h_{\mathrm{g}}^{n+1} \geq 0$ and $(hc)^{n+1} \geq 0$. Moreover,

$$z_{\mathrm{b}}^{n+1} = h_{\mathrm{m}}^{n+1} + h_{\mathrm{g}}^{n+1} = \frac{(x_0+y_0)(1+f) + w_0 f}{(1+e+f)(1-\psi_0)} \geq 0.$$

If, in addition, assumption (3.11) is in effect, then $a \geq e$, and as a consequence all terms defining h_{m}^{n+1} are nonnegative. □

3.7. **Incorporation of non-hydrostatic pressure.** The non-hydrostatic pressure is incorporated by a projection method that only affects the momentum conservation equations. Since other variables are not affected by this correction, we have

$$h^{n+1} = h^*, \quad (hc)^{n+1} = (hc)^*, \quad z_{\mathrm{b}}^{n+1} = z_{\mathrm{b}}^*, \quad h_{\mathrm{g}}^{n+1} = h_{\mathrm{g}}^n.$$

We write the semi-discrete momentum equations as

$$\begin{aligned}
(hu)^{n+1} &= (hu)^* - \Delta t\big(\partial_x(h^{n+1}q^{n+1}) + 2p_{\mathrm{nh}}^{n+1}\partial_x z_{\mathrm{b}}^{n+1}\big), \\
(hw)^{n+1} &= (hw)^* + 2\Delta t p_{\mathrm{nh}}^{n+1},
\end{aligned} \tag{3.12}$$

and inserting these expressions into the incompressibility condition (2.7b) we get the elliptic equation

$$\begin{aligned}
(h^{n+1})^2\partial_{xx}p_{\mathrm{nh}}^{n+1} + h^{n+1}\partial_x h^{n+1}\partial_x p_{\mathrm{nh}}^{n+1} + \Big(h^{n+1}\partial_{xx}(h^{n+1}+2z_{\mathrm{b}}^{n+1}) - \big(\partial_x(h^{n+1}+2z_{\mathrm{b}}^{n+1})\big)^2 - 4\Big)p_{\mathrm{nh}}^{n+1} \\
= \frac{1}{\Delta t}\big(2(hw)^* - (hu)^*\partial_x(h^{n+1}+2z_{\mathrm{b}}^{n+1}) + h^{n+1}\partial_x(hu)^*\big).
\end{aligned} \tag{3.13}$$

To numerically find the non-hydrostatic pressure values, we locate the corresponding variables at the cell interfaces $x_{i+1/2}$, and we define $p_{\mathrm{nh},i+1/2}^{n+1} \coloneqq p_{\mathrm{nh}}(x_{i+1/2}, t_{n+1})$. Then, Eq. (3.13) is discretized

at the cell interfaces as it is done in [20], where all the details are given. Once the new values of the non-hydrostatic pressure ($p_{\rm nh}^{n+1}$) are computed, the discharges are updated by using (3.12).

4. Numerical tests

4.1. **Preliminaries.** Unless otherwise specified, the following parameters will be used for the upcoming tests: $d_{\rm s} = 1.13 \times 10^{-3}\,{\rm m}$, $\psi_0 = 0.4$, $\theta_{\rm c} = 0.047$, $\rho_{\rm f} = 1000\,{\rm kg/m^3}$, $\rho_{\rm s} = 2680\,{\rm kg/m^3}$, $k_{\rm e} = 0.096$, $k_{\rm d} = 0.02$, and the Manning roughness coefficient $n = 0.02$. Furthermore, we will use the Meyer-Peter and Müller solid transport discharge for the equilibrium model case, and erosion and deposition rates given by [21] (also in [6, 18]), namely

$$D = v_{\rm s} c_{\rm b} \quad \text{and} \quad E = v_{\rm s}\psi_0 E_{\rm s},$$

where $v_{\rm s}$ is the settling velocity and $c_{\rm b}$ is the fractional concentration of suspended sediment near the bed, defined as

$$c_{\rm b} = 0.4c(d_{\rm s}/D_{\rm sg})^{1.64} + 1.64c, \tag{4.1}$$

where $D_{\rm sg}$ is the geometric mean diameter of suspended sediment particles. In the case of a single sediment type, (4.1) reduces to $c_{\rm b} = 2.04c$. Furthermore, the settling velocity is expressed as

$$v_{\rm s} = \sqrt{\left(\frac{13.95\nu}{d_{\rm s}}\right)^2 + 1.09(r_{\rm s}-1)gd_{\rm s}} - \frac{13.95\nu}{d_{\rm s}},$$

where ν is the kinematic viscosity ($\nu = 10^{-6}$) of water and $E_{\rm s}$ is the sediment entrainment coefficient, which is defined as

$$E_{\rm s} := \frac{1.3\times 10^{-7} Z^5}{1 + 4.3\times 10^{-7} Z^5} \quad \text{with} \quad Z := \begin{cases} \dfrac{\sqrt{c_{\rm D}}|u|}{v_{\rm s}}{\rm Re}^{0.6} & \text{if } {\rm Re} > 2.36, \\ 0.586\dfrac{\sqrt{c_{\rm D}}|u|}{v_{\rm s}}{\rm Re}^{1.23} & \text{if } {\rm Re} \le 2.36. \end{cases}$$

where $c_{\rm D}$ is the drag coefficient empirically defined as $c_{\rm D} = 24/{\rm Re}$, and Re is the Reynolds number for the particles:

$${\rm Re} := \frac{d_{\rm s}\sqrt{(r_{\rm s}-1)gd_{\rm s}}}{\nu}.$$

Other definitions of these terms could be used in principle (see [1, 7, 30, 33] among others).

Unless specified, hydrostatic pressure is assumed, and the stability restriction

$$\Delta t = {\rm CFL}\frac{\Delta x}{\lambda},$$

with CFL= 0.5 is used, where $\lambda = \max_i |\lambda_i|$ is the maximum eigenvalue of $\tilde{\boldsymbol{\mathcal{A}}}_{i+1/2}$ (see (3.3)) in absolute value.

The tests include several alternatives for the models in this paper: equilibrium and non-equilibrium case, with/without gravitational effects, hydrostatic/non-hydrostatic pressure, erosion-deposition effects; as well as various methods (well-balanced and non-well-balanced). First, in Test 1, we compare the results of the proposed method with exact solutions derived for the equilibrium model with gravitational effects (see [19]) and then, in Test 2, with a novel exact solution introduced here for the non-equilibrium case. Next, Test 3 is an academic test that shows how the PVM-2I scheme reduces the numerical diffusion in comparison with HLL and Rusanov methods. After that, in Tests 4 to 6, results of the equilibrium model are compared with experimental data for classical scenarios, namely overtopping flow (Test 4) and dam-break configurations (Tests 5 and 6).

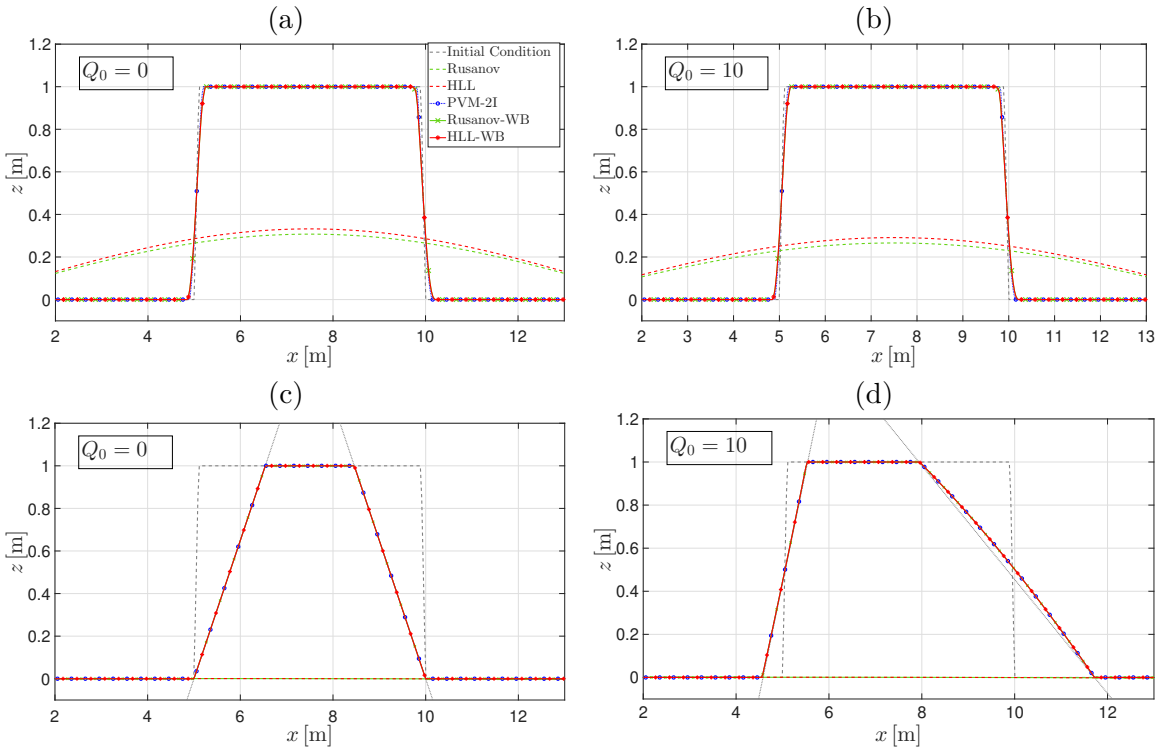

FIGURE 2. Test 1: approximate solutions $z_{\mathrm{b}}(x,t)$ for well-balanced and non-well-balanced methods (a, b) at simulated time $t = 100\,\mathrm{s}$ and (c, d) close to steady state obtained by using (a, c) $Q_0 = 0\,\mathrm{m}^2/\mathrm{s}$ and (b, d) $Q_0 = 10\,\mathrm{m}^2/\mathrm{s}$, for $\delta = 33°$.

4.2. **Test 1: sediment transport in equilibrium including gravitational effects.** We test the proposed numerical scheme for the model in equilibrium without sediment in suspension, for which an exact solution accounting for gravitational effects in simple configurations is available (see [19]). Concretely, it is proven that if $(\zeta(x), Q_0, z_{\mathrm{b}}(x))$ denote the values of the free surface, discharge, and sediment layer satisfying that $q_{\mathrm{b}} = 0$, with $Q_0 = \text{const.}$, it is a steady solution of the equilibrium model if and only if

$$-\operatorname{sgn}(\tau_{\mathrm{eff}})\beta\partial_x z_{\mathrm{b}} \leq \tan\delta\left(1 - \frac{\operatorname{sgn}(\tau_{\mathrm{eff}})C_{\mathrm{f}}|Q_0|Q_0}{g d_{\mathrm{s}}\theta_{\mathrm{c}}(r_{\mathrm{s}}-1)h^2}\right), \quad \partial_x\zeta = \alpha\partial_x z_{\mathrm{b}},$$

with $\alpha = -Q_0^2/(gh^3 - Q_0^2)$ and $\beta = 1 + \alpha/(r_{\mathrm{s}} - 1)$. As particular case, in the steady case ($Q_0 = 0$) the slope of the sediment matches the angle of repose of the material, and this steady slope varies with the constant discharge Q_0, so the slope remains stable without further erosion.

For this test, we consider the initial conditions

$$h(x,0) = 10\,\mathrm{m}, \quad hu(x,0) = Q_0\,\mathrm{m}^2/\mathrm{s}, \quad z_{\mathrm{b}}(x,0) = \begin{cases} 10\cdot(x-5)\,\mathrm{m} & \text{if } 5 < x \leq 5.1, \\ 1\,\mathrm{m} & \text{if } 5.1 < x \leq 9.9, \\ 10\cdot(10-x)\,\mathrm{m} & \text{if } 9.9 < x \leq 10, \\ 0\,\mathrm{m} & \text{otherwise,} \end{cases}$$

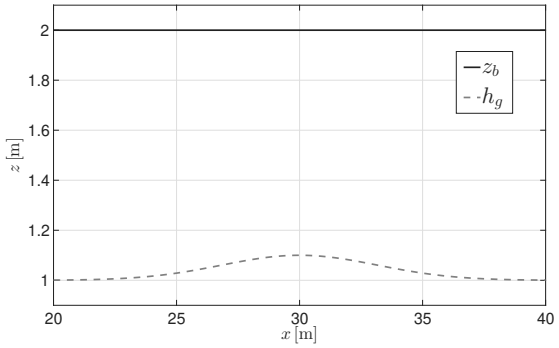

FIGURE 3. Test 2: initial condition for the erodible bed (z_b) and the fixed layer (h_g).

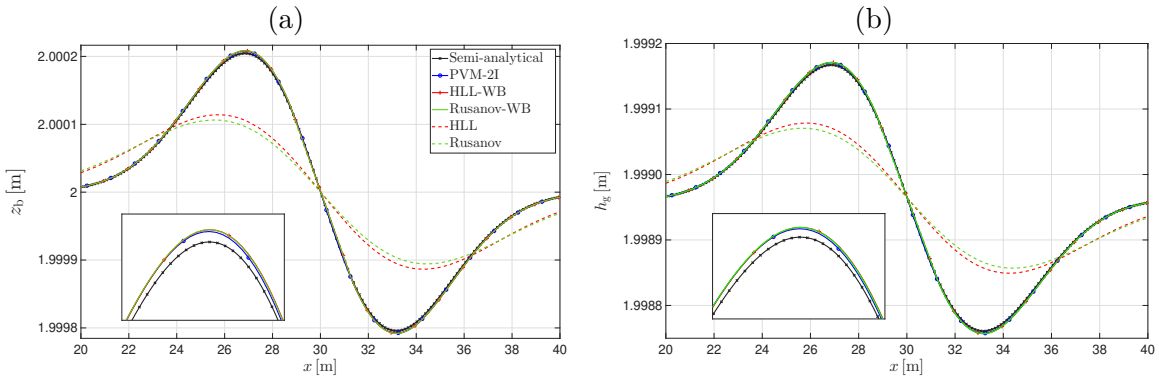

FIGURE 4. Test 2: comparisons of (a) the erodible bed z_b and (b) the fixed layer h_g for well-balanced and non-well-balanced methods at simulated time $t = 10\,\mathrm{s}$.

with a repose angle $\delta = 33^\circ$ and where Q_0 is the constant flow discharge. Two configurations will be considered, the water-at-rest case ($Q_0 = 0\,\mathrm{m}^2/\mathrm{s}$) and a constant flow $Q_0 = 10\,\mathrm{m}^2/\mathrm{s}$. The spatial domain is $[0, 15]$ m with a grid spacing $\Delta x = 0.03\,\mathrm{m}$.

Figure 2 shows the numerical results. Figures 2(a) and (b) correspond to the results after 100 s of simulated time for different schemes, when the sediment has not reached its steady state yet. The well-balanced methods behave as expected, namely they slowly approximate the exact equilibrium solution, and thereby match the performance of PVM-2I, while the non-well-balanced Rusanov and HLL schemes degrade rapidly due to numerical viscosity. Figures 2(c) and (d) show the behaviour of the PVM-2I and the well-balanced Rusanov and HLL schemes close to steady state ($t = 200000\,\mathrm{s}$). In both cases, the numerical solution reproduces properly the exact one. The expected equilibrium profile is maintained successfully. On the contrary, non-well-balanced schemes are not able to reproduce these solutions due to numerical diffusion. In fact, notice that the lines corresponding to non-well-balanced Rusanov and HLL methods are nearly flat (close to $z = 0\,\mathrm{m}$) in the plots in figures 2(c) and (d).

4.3. **Test 2: non-equilibrium model with exact solution.** Here, we consider the non-equilibrium model with no gravitational effects and derive a novel exact solution in a simplified configuration, where both the flow depth $h(x,t)$ and the velocity $u(x,t)$ remain constant in space and time.

First, we assume that there is no suspended sediment. Under these conditions, the Shields parameter $\theta(h,u)$ also remains constant, and therefore the bedload transport velocity v_b is spatially and temporally uniform. Consequently, the governing equation for the evolution of the mobile sediment layer thickness, h_m, simplifies to

$$\partial_t h_\mathrm{m} + a v_\mathrm{b} \partial_x h_\mathrm{m} = \dot{\eta}_\mathrm{e} - h_\mathrm{m} b \quad \text{with} \quad a \coloneqq \frac{\sqrt{g d_\mathrm{s}(r_\mathrm{s}-1)}}{1-\psi_0} \quad \text{and} \quad b \coloneqq \frac{\sqrt{g d_\mathrm{s}(r_\mathrm{s}-1)} k_\mathrm{d}}{d_\mathrm{s}}.$$

Previous equation is a transport equation with a source term. Its exact solution is given by

$$h_\mathrm{m}(x,t) = \frac{\dot{\eta}_\mathrm{e}}{b} + \left(h_{\mathrm{m},0}(x - a v_\mathrm{b} t) - \frac{\dot{\eta}_\mathrm{e}}{b} \right) \mathrm{e}^{-bt}.$$

being $h_{\mathrm{m},0}(x) = h_\mathrm{m}(x,0)$ the initial condition. Thus, the term $h_{\mathrm{m},0}(x - a v_\mathrm{b} t)$ represents a wave propagating through the domain with velocity $a v_\mathrm{b}$. Roughly speaking, this wave propagates much more slowly than the rate at which its amplitude decays due to the exponential term. Furthermore, if $\theta \leq \theta_\mathrm{c}$, and hence $\dot{\eta}_\mathrm{e} = 0$, the wave remains stationary. The solution is exact under the assumption that $h(x,t)$, $u(x,t)$, $z_\mathrm{b}(x,t)$, and $h_{\mathrm{m},0}(x)$ remain constant. However, if $h_{\mathrm{m},0}(x)$ varies in space we get a semi-analytical solution. Actually, a non-uniform function $h_{\mathrm{m},0}(x)$ leads to a non-constant bed elevation $z_\mathrm{b}(x,t)$ given by the solution of

$$\partial_t z_\mathrm{b} = -a v_\mathrm{b} \partial_x h_\mathrm{m}.$$

Thus, variations in $h_{\mathrm{m},0}(x)$ induce deviations in $z_\mathrm{b}(x,t)$, and consequently, $h(x,t)$ and $u(x,t)$ are no longer strictly constant but small perturbations appear.

On the other hand, regardless of the initial condition $h_{\mathrm{m},0}(x)$, the system evolves towards an equilibrium state as $t \to \infty$, given by

$$h_\mathrm{m} = \frac{k_\mathrm{e}}{1-\psi_0} \frac{d_\mathrm{s}}{k_\mathrm{d}} (\theta - \theta_\mathrm{c})_+.$$

This implies that in the long time, the mobile sediment layer thickness stabilizes according to the equilibrium entrainment and deposition dynamics.

The solutions for the immobile sediment layer thickness h_g and bed elevation z_b are given by

$$\begin{aligned} h_\mathrm{g}(x,t) &= h_{\mathrm{g},0}(x) + \frac{\dot{\eta}_\mathrm{e}}{b}(\mathrm{e}^{-bt} - 1) + b \int_0^t h_{\mathrm{m},0}(x - a v_\mathrm{b} \tau) \mathrm{e}^{-b\tau} \, \mathrm{d}\tau, \\ z_\mathrm{b}(x,t) &= h_{\mathrm{g},0}(x) + h_{\mathrm{m},0}(x - a v_\mathrm{b} t) \mathrm{e}^{-bt} + b \int_0^t h_{\mathrm{m},0}(x - a v_\mathrm{b} \tau) \mathrm{e}^{-b\tau} \, \mathrm{d}\tau. \end{aligned}$$

with $h_{\mathrm{g},0}(x) = h_\mathrm{g}(x,0)$. Assuming $a v_\mathrm{b} \ll b$, we approximate $h_{\mathrm{m},0}(x - a v_\mathrm{b} t) \approx h_{\mathrm{m},0}(x)$, which yields

$$\begin{aligned} h_\mathrm{g}(x,t) &= h_{\mathrm{g},0}(x) + \left(h_{\mathrm{m},0}(x) - \frac{\dot{\eta}_\mathrm{e}}{b} \right) (1 - \mathrm{e}^{-bt}) + \mathcal{O}(a v_\mathrm{b}), \\ z_\mathrm{b}(x,t) &= z_{\mathrm{b},0}(x) + \mathcal{O}(a v_\mathrm{b}/b), \end{aligned}$$

where $z_{\mathrm{b},0}(x) \coloneqq h_{\mathrm{g},0}(x) + h_{\mathrm{m},0}(x)$. This result suggests that z_b remains almost constant over time. By integrating by parts, we can further refine the solution. By using

$$b \int_0^t h_{\mathrm{m},0}(x - a v_\mathrm{b} \tau) \mathrm{e}^{-b\tau} \, \mathrm{d}\tau = -h_{\mathrm{m},0}(x - a v_\mathrm{b} \tau) \mathrm{e}^{-b\tau} \Big|_0^t - a v_\mathrm{b} \int_0^t h'_{m,0} \mathrm{e}^{-b\tau} \, \mathrm{d}\tau,$$

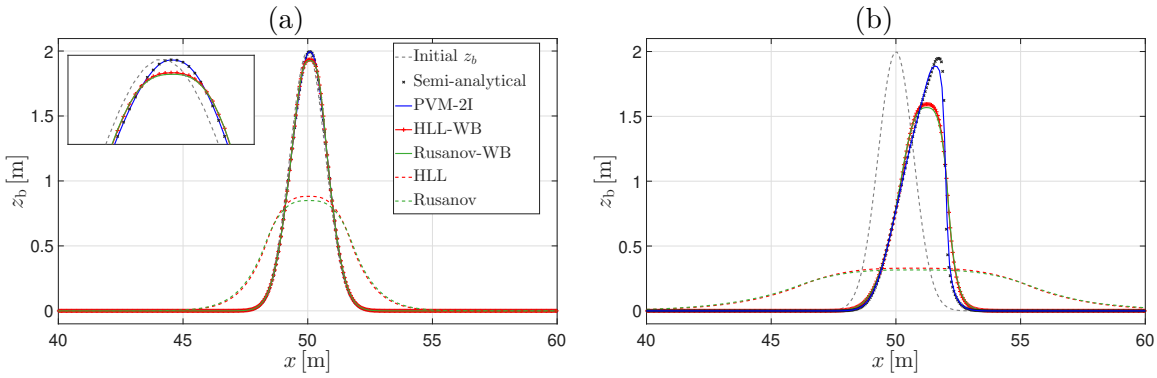

FIGURE 5. Test 3: solutions of the erodible bed (z_b) for well-balanced and non-well-balanced methods at simulated times (a) $t = 100\,\mathrm{s}$ and (b) $t = 2000\,\mathrm{s}$.

where $h'_{\mathrm{m},0} \coloneqq \mathrm{d}h_{\mathrm{m},0}/\mathrm{d}z$ with $z = x - av_\mathrm{b}t$, and again assuming $av_\mathrm{b} \ll b$, we obtain the first-order correction

$$h_\mathrm{g}(x,t) = h_{\mathrm{g},0}(x) + \left(h_{\mathrm{m},0}(x) - \frac{\dot\eta_\mathrm{e}}{b} - \frac{av_\mathrm{b}}{b}h'_{\mathrm{m},0}(x)\right)(1 - \mathrm{e}^{-bt}) + \mathcal{O}((av_\mathrm{b}/b)^2),$$
$$z_\mathrm{b}(x,t) = z_{\mathrm{b},0}(x) - \frac{av_\mathrm{b}}{b}h'_{\mathrm{m},0}(1 - \mathrm{e}^{-bt}) + \mathcal{O}((av_\mathrm{b}/b)^2).$$

These corrections might be systematically improved by iterating the integration-by-parts process.

In the case of sediment in suspension, which is not considered in this test, the solution generalizes as

$$h_\mathrm{m}(x,t) = \frac{d}{b} + \left(h_{\mathrm{m},0}(x - av_\mathrm{b}t) - \frac{d}{b}\right)\mathrm{e}^{-bt}$$

with

$$a \coloneqq \frac{\sqrt{gd_\mathrm{s}(r_\mathrm{s}-1)}}{1-\psi_0}, \quad b \coloneqq \frac{\sqrt{gd_\mathrm{s}(r_\mathrm{s}-1)}k_\mathrm{d}}{d_\mathrm{s}}, \quad \text{and} \quad d \coloneqq \dot\eta_\mathrm{e} - \frac{E-D}{1-\psi_0}.$$

We test the numerical scheme for the case with no suspended sediment and with initial conditions

$$h(x,0) = 8\,\mathrm{m}, \quad hu(x,0) = 10\,\mathrm{m}^2/\mathrm{s}, \quad z_\mathrm{b}(x,0) = 2\,\mathrm{m}, \quad h_\mathrm{g}(x,0) = 1 + \frac{1}{10}e^{-\frac{(x-30)^2}{20}}\,\mathrm{m}$$

We consider the domain $[0, 60]\,\mathrm{m}$ with $\Delta x = 0.1\,\mathrm{m}$. This is a fast test, so $t = 10\,\mathrm{s}$ is sufficient time to study the behaviour of the solution and the schemes. The initial condition for z_b and h_g is depicted in Figure 3, and Figure 4 shows the comparison between semi-analytical and numerical solutions at $t = 10\,\mathrm{s}$. We see that the solutions of PVM-2I scheme and the well-balanced versions of HLL and Rusanov methods are in close agreement, demonstrating the accuracy of the numerical schemes. On the contrary, non-well-balanced methods exhibit non-physical erosion and fail to reach a steady state. The solution continues to erode on time, eventually flattening the bottom completely.

4.4. **Test 3: "academic" dune transport.** We highlight the accuracy of the PVM-2I scheme and the importance of using well-balanced methods by a simple academic test such as the transport of a simple dune. Moreover, under the assumption $h \gg z_\mathrm{b}$, one may assume the equilibrium regime for the system and

$$h = A - z_\mathrm{b}, \quad \text{and} \quad hu = \text{const.},$$

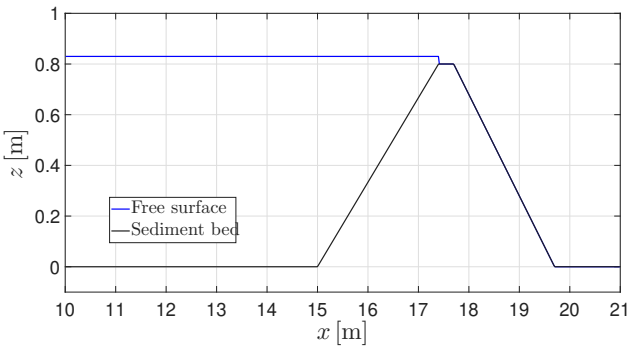

FIGURE 6. Test 4: initial condition for the free surface ($z_\mathrm{b} + h$) and sediment bed (z_b) in the experiment of [34].

where $A \in \mathbb{R}$ is a constant such that $A > z_\mathrm{b}$. These expressions can be replaced in the equations for z_b and h_g, which are subsequently solved numerically. So, we get an approximate semi-analytical solution. It is important to remark that the modified system exhibits eigenvalues that differ from the original ones.

Here we consider the initial conditions

$$h(x,0) = 10 - z_\mathrm{b}(x,0)\ \mathrm{m}, \quad hu(x,0) = 10\,\mathrm{m}^2/\mathrm{s}, \quad z_\mathrm{b}(x,0) = 2e^{-(x-50)^2}\ \mathrm{m},$$

and the Manning coefficient is taken here as $n = 0.05$ to increase the transport rate and exhibit the differences between the various schemes. The simulation domain spans $[0, 100]$ m with spatial resolution $\Delta x = 0.02$ m.

Figure 5 shows the dune evolution at simulated times $t = 100$ s and $t = 2000$ s along with the approximate semi-analytical solution. On the one hand, the numerical solution of the PVM-2I scheme is the closest to the semi-analytical reference solution. This property highlights its accuracy to reproduce the sediment evolution compared to the well-balanced Rusanov and HLL schemes, where we recall that these schemes are identical for the equations of fluid variables. We observe that the non-well-balanced schemes do not reproduce these solutions as a consequence of numerical diffusion. This behaviour lends further support to the proposed well-balanced correction and serves as a strong validation of the proposed PVM-2I scheme for such problems. On the other hand, the schemes Rusanov-WB and HLL-WB, although they are more diffusive than PVM-2I, acceptably approximate the dune evolution. The main advantage of the Rusanov-WB and HLL-WB schemes is that they are conceptually simpler and accurate methods, and therefore both are potential candidates for the construction of high-order methods when combined with high-order techniques such as reconstruction of states (see [9]).

4.5. **Test 4: overtopping flow erosion.** We now compare our numerical results with experimental data in [34] for a overtopping flow erosion process. The experimental setup consists of a rectangular channel of length 30 m and width 0.3 m wide including a trapezoidal sediment dam. A constant incoming flow (1.23 liters per second) is imposed upstream, and the flow starts to erode the sediment bed. Erosion/deposition effects are not considered here so that we may directly compare the effects of numerical dissipation over erosion. It is worth mentioning that some references apply the sediment transport but not erosion/deposition while others consider just erosion/deposition effects; cf., e.g., [2, 26].

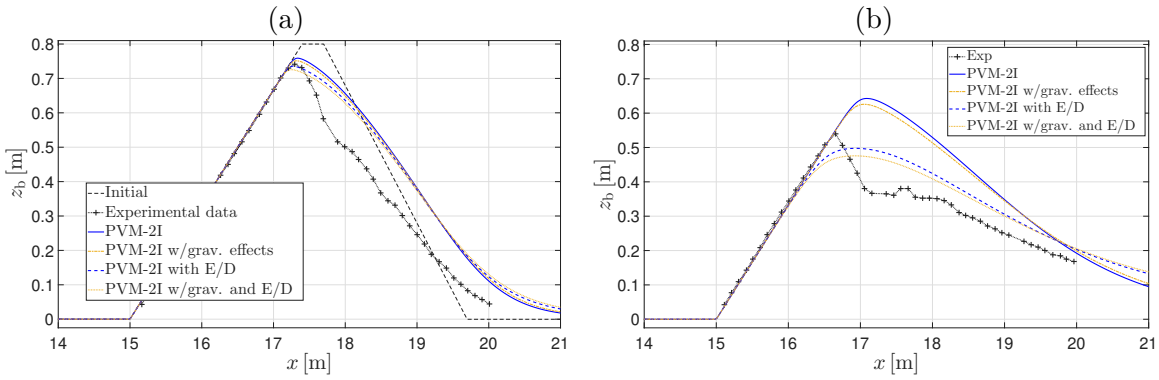

FIGURE 7. Test 4: comparison of experimental data of bed evolution (black with symbols lines) ([34]) at (a) $t = 30\,\mathrm{s}$ and (b) $t = 60\,\mathrm{s}$ with results of the equilibrium model with PVM-2I method with and without erosion/deposition (E/D) terms (dashed and continuous lines, respectively), with and without gravitational effects (brown and blue lines, respectively).

As domain we take $[0, 25]\,\mathrm{m}$ with $\Delta x = 0.01\,\mathrm{m}$, and the initial conditions (see Figure 6) are given by

$$h(x,0) = \begin{cases} 0.83\,\mathrm{m} & \text{if } x \le 17.4, \\ 0\,\mathrm{m} & \text{if } x > 17.4. \end{cases}, \quad hu(x,0) = 1.23 \times 10^{-3}\,\mathrm{m}^2/\mathrm{s},$$

$$z_\mathrm{b}(x,0) = \begin{cases} (x-15)/3\,\mathrm{m} & \text{if } 15 < x \le 17.4, \\ 0.8\,\mathrm{m} & \text{if } 17.4 < x \le 17.7, \\ 0.8 + (x-17.7)/2.5\,\mathrm{m} & \text{if } 17.7 < x < 19.7, \\ 0\,\mathrm{m} & \text{otherwise.} \end{cases}$$

In this case, we use the porosity $\psi_0 = 0.35$ and the Manning roughness coefficient $n = 0.015$. We compare here the results of the equilibrium model.

For this test, gravitational effects do not have a significant influence on the results, as it is shown in Figure 7. This outcome is partly due to the choice of the test slope smaller than the repose angle of 25°, which reduces the influence of gravitational forces on the overall behaviour of the system.

In Figure 8(b) the influence of erosion and deposition (E/D) terms is depicted. We observe that the results are close to the experimental data when erosion/deposition terms are activated. Figure 8(c) shows a comparison between the standard Rusanov and HLL solvers and their well-balanced versions as well as PVM-2I scheme for the model without erosion/deposition terms. As it is shown, the standard Rusanov and HLL methods produce a faster erosion than the well-balanced versions. This indicates the presence of non-physical erosion in some regions. Although this additional erosion might locally resemble the experimental data at $t = 60\,\mathrm{s}$, it is incorrect and cannot be controlled.

4.6. **Tests 5 and 6: dam-break problems.** In these tests, we reproduce some dam-break experiments reported in [8] and [31]. Dam-break test cases, such as the ones performed here, involve rapid erosion, and conventional sediment transport formulations usually do not properly capture its dynamics. For this reason, we omit the sediment transport (advection) term from the equations ($q_\mathrm{b} = 0$) in these tests, which allows us to isolate and analyse the contribution of local bed changes driven solely by erosion and deposition.

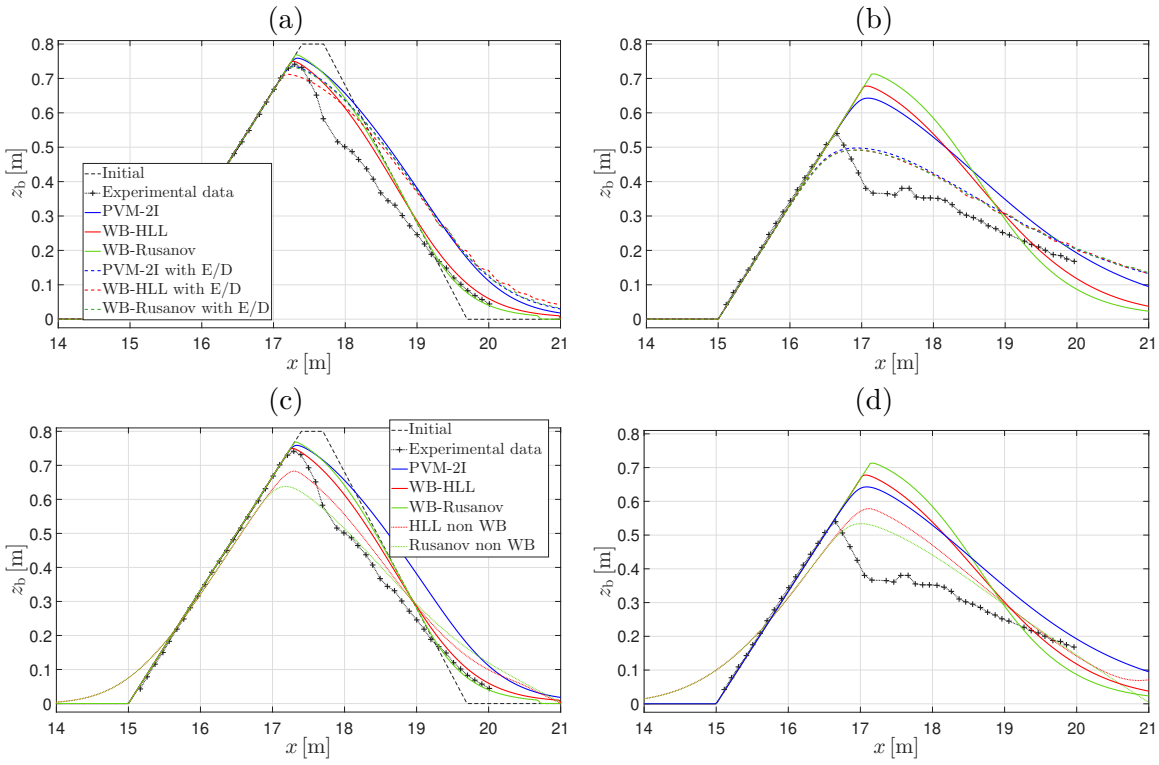

FIGURE 8. Test 4: Comparison of bed evolution experimental data (black with symbols lines) ([34]) at (a, c) $t = 30\,\mathrm{s}$ and (b, d) $t = 60\,\mathrm{s}$ with results of the equilibrium model with PVM-2I, Rusanov, and HLL methods (blue, green, and red lines, respectively). Plots (a, b): comparison of the results with and without erosion/deposition (E/D) terms (dashed and continuous lines); plots (c, d): comparison of the results of well-balanced and non-well-balanced numerical methods (dashed and continuous lines, respectively).

Test 5 is based on the experiments conducted in [8] that correspond to the initial condition

$$h(x,0) = \begin{cases} 0.1\,\mathrm{m} & \text{if } x \leq 0, \\ 0\,\mathrm{m} & \text{otherwise.} \end{cases}, \quad z_\mathrm{b}(x,0) = 0\,\mathrm{m}, \quad hu(x,0) = 0\,\mathrm{m}^2/\mathrm{s}, \quad c(x,0) = 0.$$

The test configuration is a dam break over a low density sediment bottom. The parameters are the fluid density $\rho = 1000\,\mathrm{kg/m^3}$, the sediment density $\rho_\mathrm{s} = 1048\,\mathrm{kg/m^3}$, and the particle diameter $d = 6.1 \times 10^{-3}\,\mathrm{m}$. Gravitational effects are not included in this test, as their influence on the results was found to be negligible. We focus on the influence of non-hydrostatic effects on the results. The computational domain $[-1, 1]\,\mathrm{m}$ is discretized using a uniform grid spacing $\Delta x = 0.001\,\mathrm{m}$.

Figure 9 shows the comparison between simulations with and without non-hydrostatic pressure and experimental measurements. As it is observed, the inclusion of non-hydrostatic pressure improves slightly the ability of the model to capture the physical behaviour of the flow, in particular the water level. Notice that the effect of non-hydrostatic pressures becomes more significant over time; initially, the impact is minimal, but it becomes more pronounced at later stages.

Test 6 is related to a similar experiment setup presented in [31]. In this experiment, the sediment properties are $d_\mathrm{s} = 3.9 \times 10^{-3}\,\mathrm{m}$, $\rho_\mathrm{s} = 1580\,\mathrm{kg/m^3}$, and porosity $\psi_0 = 0.47$. The roughness coefficient is specified as $n = 0.0165$. The simulation was carried out for a total time of $T_\mathrm{f} = 1.5\,\mathrm{s}$.

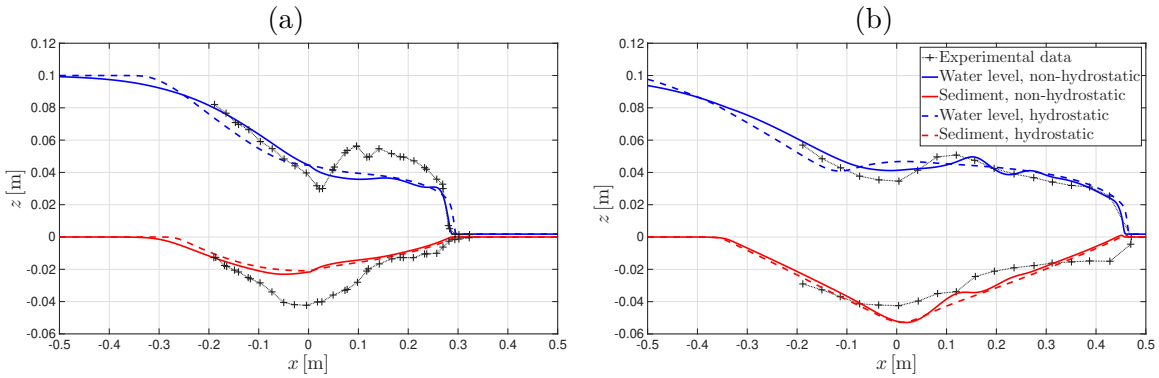

FIGURE 9. Test 5: comparison between experimental data [8] and numerical results for models with hydrostatic and non-hydrostatic pressure at simulated times (a) $t = 3t_0$ and (b) $t = 5t_0$, where $t_0 = \sqrt{h_0/g}$ and h_0 is the initial water level before the dam break.

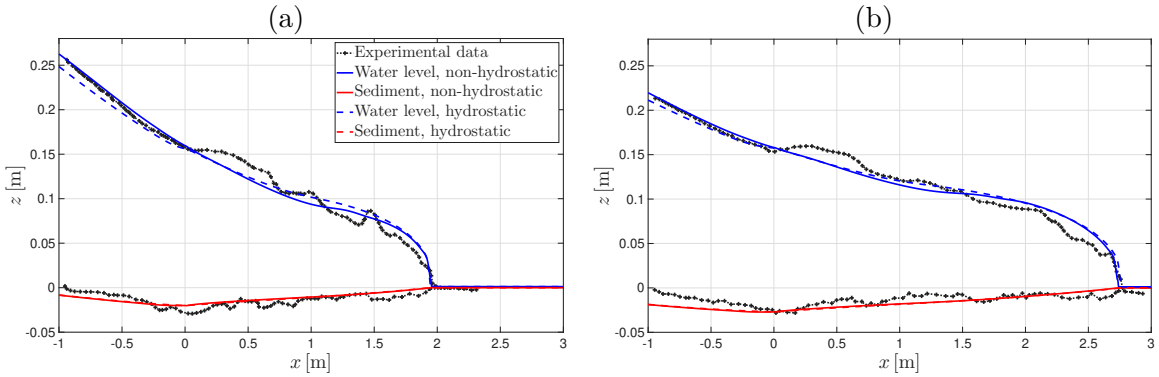

FIGURE 10. Test 6: comparison between experimental data ([31]) and numerical results for models with hydrostatic and non-hydrostatic pressure at simulated times (a) $t = 1\,\mathrm{s}$ and (b) and $t = 1.5\,\mathrm{s}$.

The computational domain for this experiment is defined as $[-3, 3]\,\mathrm{m}$, which is discretized with $\Delta x = 0.001\,\mathrm{m}$. The initial conditions are given by

$$h(x,0) = \begin{cases} 0.35\,\mathrm{m} & \text{if } x \le 0, \\ 0\,\mathrm{m} & \text{otherwise.} \end{cases} \qquad hu(x,0) = 0\,\mathrm{m}^2/\mathrm{s}, \quad c(x,0) = 0, \quad z_\mathrm{b}(x,0) = 0\,\mathrm{m}.$$

Figure 10 shows only minor differences between the model with and without non-hydrostatic pressure at both time steps. While bottom erosion appears nearly identical in both cases, the non-hydrostatic model captures the water level slightly more accurately on the left side.

5. CONCLUSIONS

A simplified depth-averaged model for sediment transport has been proposed. The model incorporates the suspended sediment concentration in the fluid, bedload transport, and erosion and deposition rates between the moving and the static granular layers. Moreover, gravitational effects in the sediment bed and non-hydrostatic pressure for the fluid are included. Its deduction is based on the Boussinesq hypothesis and the limit approximation of sediment concentration when

approaching to the sediment-water interface. The final model satisfies a dissipative energy balance. Since a general formulation has been employed, the model can be considered either in equilibrium (erosion rate equals deposition rate) or non-equilibrium conditions.

All stages of the formulation of numerical scheme, corresponding to all physical effects, are detailed for completeness. The main contribution of the paper concerns the design of well-balanced schemes for SVE models. Usually, well-balanced schemes are focused on water-at-rest solutions for Saint-Venant systems with a fixed bottom. However, these schemes are in general no more well-balanced when they are applied to SVE models since the numerical diffusion for the sediment bed remains uncontrolled, and therefore the sediment is not steady. In particular, this holds for the common Rusanov and HLL schemes. Here, two strategies are proposed: (i) a novel PVM-2I method that can be seen as the combination of the HLL method for the fluid and a second-order PVM method for the sediment, which accounts for the intermediate wave speed corresponding to the sediment layer, and it is well-balanced for SVE model by construction; (ii) a correction of Rusanov and HLL methods in terms of the Shields parameter that makes them well-balanced for the SVE model. This procedure is physically motivated from the derivation of equilibrium case, in the sense that the definition of the mobile sediment bed in equilibrium is used for the numerical discretization of the non-equilibrium model.

Several numerical tests are performed to validate the model and the new well-balanced numerical schemes. In particular, a novel semi-analytical solution for the non-equilibrium model case is introduced (see Subsection 4.3), which is useful to validate the model and the schemes. After some academic tests, where we show that the PVM-2I method is less diffusive than the Rusanov and HLL methods (see Test 3), comparisons with experimental data for overtopping flow erosion and dam break configurations are performed. We have seen that gravitational effects play a key role to preserve steady states with physical meaning (see Test 1), whereas they have a small influence in other cases, as in overtopping flow erosion experiments (Test 4).

Concerning the overtopping flow erosion test (Test 4) we show that non-well-balanced methods are more accurate than well-balanced methods because of the uncontrolled numerical diffusion. So, it is important to point out that this cannot be considered as correct despite of being closer to the experimental data. Rather, results suggest that the model should be improved in order to reproduce these experimental data. We have also shown that considering erosion and deposition terms between the bedload layer and the sediment concentrations in the fluid improves greatly the results in comparison with experimental data.

We also study the influence of non-hydrostatic pressure in the fluid for two dam-break problems (Tests 5 and 6), where the non-hydrostatic effects improve the results of the water surface. In this test, we have only considered erosion/deposition effects and not bedload transport, since the combination of both produces too much erosion. Note that for this test there is a strong fluid-sediment interaction. This scenario is far from the assumptions made to derive classical solid transport discharge formulas in SVE models.

As final conclusion, we point out that, up to our knowledge, this is the first time that well-balanced versions of Rusanov and HLL methods have been proposed for Saint-Venant-Exner type models. Furthermore, their extensions to high-order methods should be straightforward by using high-order state reconstructions techniques, which is a future extension of this work.

Acknowledgements

This research has been partially supported by Junta de Andalucía research project ProyExcel_00525 and by the European Union - NextGenerationEU program and by grant PID2022-137637NB-C22 funded by MCIN/AEI/10.13039/501100011033 and "ERDF A way of making Europe". R.B. is supported by ANID (Chile) through Fondecyt project 1250676, Centro de Modelamiento Matemático CMM (BASAL project FB210005), and CRHIAM, project ANID/ FONDAP/ 1523A0001. J.M. supported by ANID scholarship ANID-PCHA/Doctorado Nacional/2021-21211457 and the regional Andalusian Government I+D+i PAIDI 2021 project ProyExcel_00525.

References

[1] J. Akiyama and Y. Fukushima. Entrainment of noncohesive bed sediment into suspension. Technical Report External Memo. No. 175, Minneapolis, USA, 1985.

[2] A. Al-Ghosoun, M. Seaid, and A. S. Osman. A novel approach for modelling stress fields induced by shallow water flows on movable beds. Applied Mathematical Modelling, 142:115960, 2025.

[3] K. Ashida and M. Michiue. Study on hydraulic resistance and bed-load transport rate in alluvial streams. Proceedings of the Japan Society of Civil Engineers, 1972(206):59–69, 1972.

[4] Y. Bai and K. F. Cheung. Depth-integrated free-surface flow with a two-layer non-hydrostatic formulation. International Journal for Numerical Methods in Fluids, 69(2):411–429, 2011.

[5] F. Bouchut. Nonlinear Stability of Finite Volume Methods for Hyperbolic Conservation Laws. Birkhäuser Basel, June 2004.

[6] S. F. Bradford and N. D. Katopodes. Hydrodynamics of turbid underflows. I: Formulation and numerical analysis. Journal of Hydraulic Engineering, 125(10):1006–1015, Oct. 1999.

[7] Z. Cao, G. Pender, S. Wallis, and P. Carling. Computational dam-break hydraulics over erodible sediment bed. Journal of Hydraulic Engineering, 130(7):689–703, July 2004.

[8] H. Capart and D. L. Young. Formation of a jump by the dam-break wave over a granular bed. Journal of Fluid Mechanics, 372:165–187, Oct. 1998.

[9] M. Castro, J. M. Gallardo, and C. Parés. High order finite volume schemes based on reconstruction of states for solving hyperbolic systems with nonconservative products. Applications to shallow-water systems. Mathematics of Computation, 75(255):1103–1135, mar 2006.

[10] M. J. Castro, T. Morales de Luna, and C. Parés. Well-Balanced Schemes and Path-Conservative Numerical Methods. In R. Abgrall and C.-W. Shu, editors, Handbook of Numerical Analysis, volume 18 of Handbook of Numerical Methods for Hyperbolic Problems Applied and Modern Issues, pages 131–175. Elsevier, 2017. DOI: 10.1016/bs.hna.2016.10.002.

[11] M. J. Castro Díaz and E. D. Fernández-Nieto. A class of computationally fast first order finite volume solvers: PVM methods. SIAM Journal on Scientific Computing, 34(4):A2173–A2196, jan 2012.

[12] G. Dal Maso, P. G. Lefloch, and F. Murat. Definition and weak stability of nonconservative products. Journal de mathématiques pures et appliquées, 74(6):483–548, 1995.

[13] C. Escalante and T. Morales de Luna. A general non-hydrostatic hyperbolic formulation for boussinesq dispersive shallow flows and its numerical approximation. Journal of Scientific Computing, 83(3), jun 2020.

[14] C. Escalante Sánchez, E. D. Fernández-Nieto, T. Morales de Luna, Y. Penel, and J. Sainte-Marie. Numerical simulations of a dispersive model approximating free-surface Euler equations. Journal of Scientific Computing, 89(3), oct 2021.

[15] F. M. Exner. Zur Physik der Dünen. Hölder, Wien, Austria, 1920.

[16] E. D. Fernández-Nieto, T. Morales de Luna, G. Narbona-Reina, and J. D. Zabsonré. Formal deduction of the Saint-Venant–Exner model including arbitrarily sloping sediment beds and associated energy. ESAIM: Mathematical Modelling and Numerical Analysis, 51(1):115–145, 2017.

[17] E. D. Fernández-Nieto, M. Parisot, Y. Penel, and J. Sainte-Marie. A hierarchy of dispersive layer-averaged approximations of Euler equations for free surface flows. Communications in Mathematical Sciences, 16(5):1169–1202, 2018.

[18] M. Garcia and G. Parker. Experiments on the entrainment of sediment into suspension by a dense bottom current. Journal of Geophysical Research: Oceans, 98(C3):4793–4807, Mar. 1993.

[19] J. Garres-Díaz, E. Fernández-Nieto, and G. Narbona-Reina. A semi-implicit approach for sediment transport models with gravitational effects. Applied Mathematics and Computation, 421:126938, May 2022.

[20] J. Garres-Díaz, E. D. Fernández-Nieto, A. Mangeney, and T. Morales de Luna. A weakly non-hydrostatic shallow model for dry granular flows. Journal of Scientific Computing, 86(2), jan 2021.
[21] J. C. González-Aguirre, M. J. Castro, and T. Morales de Luna. A robust model for rapidly varying flows over movable bottom with suspended and bedload transport: Modelling and numerical approach. Advances in Water Resources, 140:103575, 2020.
[22] E. Guerrero Fernández, M. Castro Díaz, Y. Wei, and C. Moore. Modeling sediment movement in the shallow-water framework: A morpho-hydrodynamic approach with numerical simulations and experimental validation. Ocean Modelling, 192:102445, Dec. 2024.
[23] A. Harten, P. D. Lax, and B. van Leer. On upstream differencing and Godunov-type schemes for hyperbolic conservation laws. SIAM Rev., 25(1):35–61, 1983.
[24] R. J. LeVeque. Finite volume methods for hyperbolic problems. Cambridge Texts in Applied Mathematics. Cambridge University Press, Cambridge, 2002.
[25] X. Liu, A. Mohammadian, A. Kurganov, and J. A. Infante Sedano. Well-balanced central-upwind scheme for a fully coupled shallow water system modeling flows over erodible bed. Journal of Computational Physics, 300:202–218, 2015.
[26] S. Martínez-Aranda, J. Fernández-Pato, and P. García-Navarro. Non-equilibrium bedload transport model applied to erosive overtopping dambreach. Water, 15(17):3094, Aug. 2023.
[27] E. Meyer-Peter and R. Müller. Formulas for bed-load transport. Rep. 2nd Meet. Int. Assoc. Hydraul. Struct. Res., Stockholm, page 39–64, 1948.
[28] C. Parés. Numerical methods for nonconservative hyperbolic systems: a theoretical framework. SIAM Journal on Numerical Analysis, 44(1):300–321, jan 2006.
[29] C. Parés and M. Castro. On the well-balance property of Roe's method for nonconservative hyperbolic systems. Applications to shallow-water systems. ESAIM: Mathematical Modelling and Numerical Analysis, 38(5):821–852, sep 2004.
[30] J. Richardson and W. Zaki. Sedimentation and fluidisation: Part I. Chemical Engineering Research and Design, 75:S82–S100, Dec. 1997.
[31] B. Spinewine and Y. Zech. Small-scale laboratory dam-break waves on movable beds. Journal of Hydraulic Research, 45(sup1):73–86, dec 2007.
[32] P. K. Stansby and J. G. Zhou. Shallow-water flow solver with non-hydrostatic pressure: 2D vertical plane problems. International Journal for Numerical Methods in Fluids, 28(3):541–563, 1998.
[33] G. Tan, H. Fang, S. Dey, and W. Wu. Rui-Jin Zhang's research on sediment transport. Journal of Hydraulic Engineering, 144(6), June 2018.
[34] T. Tingsanchali and C. Chinnarasri. Numerical modelling of dam failure due to flow overtopping. Hydrological Sciences Journal, 46(1):113–130, Feb. 2001.
[35] I. Toumi. A weak formulation of Roe's approximate Riemann solver. J. Comput. Phys., 102(2):360–373, 1992.
[36] G. Wei, J. Kirby, S. Grilli, and R. Subramanya. A fully nonlinear Boussinesq model for surface waves. Part 1. Highly nonlinear unsteady waves. Journal of Fluid Mechanics, 294(-1):71, 1995.
[37] C. H. Wu, C.-C. Young, Q. Chen, and P. J. Lynett. Efficient nonhydrostatic modeling of surface waves from deep to shallow water. Journal of Waterway, Port, Coastal, and Ocean Engineering, 136(2):104–118, 2010.
[38] Y. Yamazaki, Z. Kowalik, and K. Cheung. Depth-integrated, non-hydrostatic model for wave breaking and run-up. Numerical Methods in Fluids, 61:473–497, 2008.

Centro de Investigación en Ingeniería Matemática (CI^{2}MA)

PRE-PUBLICACIONES 2025

2025-07 Aníbal Coronel, Fernando Huancas, Mauricio Sepúlveda: *Theoretical and numerical approaches of reaction term identification in a SIS reaction diffusion system*

2025-08 Isaac Bermudez, Gabriel N. Gatica, Juan P. Silva: *A new Banach spaces-based mixed finite element method for the coupled Navier-Stokes and Darcy equations*

2025-09 Sergio Caucao, Gabriel N. Gatica, Saulo Medrado, Yuri D. Sobral: *A posteriori error analysis of mixed finite element methods for a regularized mu(I)-rheology model of granular materials*

2025-10 Veronica Anaya, Gerardo Chowell, Felipe Jara, Mauricio Sepúlveda: *Optimal control of inter-population disease spread via reaction–diffusion models*

2025-11 Ramiro Acevedo, Rommel Bustinza, Christian Gómez: *A transient Eddy current problem via potential formulation with current excitation*

2025-12 Abraham J. Arenas, Juan Barajas-Calonge, Gilberto González-Parra, Luis M. Villada: *A second-order nonstandard finite difference scheme for eco-epidemiological predator-prey models*

2025-13 Alonso J. Bustos, Sergio Caucao, Gabriel N. Gatica: *Mixed-primal and fully-mixed formulations for the convection-diffusion-reaction system based upon Brinkman–Forchheimer equations*

2025-14 Gabriel N. Gatica, Zeinab Gharibi, Ricardo Oyarzúa: *Banach spaces-based fully mixed finite element methods for the n-dimensional Boussinesq problem with temperature-dependent parameters*

2025-15 Sergio Caucao, Ricardo Oyarzúa, Segundo Villa-Fuentes: *A priori and a posteriori error analyses of a fully-mixed finite element method for the coupled Navier Stokes / Darcy problem*

2025-16 Juan Barajas-Calonge, Raimund Bürger, Pep Mulet, Luis M. Villada: *A second-order invariant-region-preserving scheme for a transport-flow model of polydisperse sedimentation*

2025-17 Raimund Bürger, Stefan Diehl, María Carmen Martí, Yolanda Vásquez: *A numerical scheme for a model of a flotation column including the transport of liquid components*

2025-18 Raimund Bürger, Enrique D. Fernández Nieto, José Garres-Díaz, Jorge Moya: *Well-balanced physics-based finite volume schemes for Saint-Venant-Exner-type models of sediment transport*

Para obtener copias de las Pre-Publicaciones, escribir o llamar a: Director, Centro de Investigación en Ingeniería Matemática, Universidad de Concepción, Casilla 160-C, Concepción, Chile, Tel.: 41-2661324, o bien, visitar la página web del centro: http://www.ci2ma.udec.cl







Centro de Investigación en
Ingeniería Matemática (CI²MA)
Universidad de Concepción

Casilla 160-C, Concepción, Chile
Tel.: 56-41-2661324/2661554/2661316
http://www.ci2ma.udec.cl